The purine nucleoside phosphorylase *pnp-1* regulates epithelial cell resistance to infection in *C. elegans*

Short running title: Purine metabolism regulates epithelial immunity

Eillen Tecle[1], Crystal B. Chhan[1], Latisha Franklin[2], Ryan S. Underwood[1], Wendy Hanna-Rose[2], and Emily R. Troemel*[1]

1 Division of Biological Sciences, University of California, San Diego, La Jolla, California, United States of America

2 Department of Biochemistry and Molecular Biology, The Pennsylvania State University, University Park, Pennsylvania, United States of America

*Corresponding author

Email: etroemel@ucsd.edu

Abstract

Intestinal epithelial cells are subject to attack by a diverse array of microbes, including intracellular as well as extracellular pathogens. While defense in epithelial cells can be triggered by pattern recognition receptor-mediated detection of microbe-associated molecular patterns, there is much to be learned about how they sense infection via perturbations of host physiology, which often occur during infection. A recently described host defense response in the nematode *C. elegans* called the Intracellular Pathogen Response (IPR) can be triggered by infection with diverse natural intracellular pathogens, as well as by perturbations to protein homeostasis. From a forward genetic screen, we identified the *C. elegans* ortholog of purine nucleoside phosphorylase *pnp-1* as a negative regulator of IPR gene expression, as well as a negative regulator of genes induced by extracellular pathogens. Accordingly, *pnp-1* mutants have resistance to both intracellular and extracellular pathogens. Metabolomics analysis indicates that *C. elegans pnp-1* likely has enzymatic activity similar to its human ortholog, serving to convert purine nucleosides into free bases. Classic genetic studies have shown how mutations in human purine nucleoside phosphorylase cause immunodeficiency due to T-cell dysfunction. Here we show that *C. elegans pnp-1* acts in intestinal epithelial cells to regulate defense. Altogether, these results indicate that perturbations in purine metabolism are likely monitored as a cue to promote defense against epithelial infection in the nematode *C. elegans*.

Author summary

All life requires purine nucleotides. However, obligate intracellular pathogens are incapable of generating their own purine nucleotides and thus have evolved strategies to steal these nucleotides from host cells in order to support their growth and replication. Using the small roundworm *C. elegans*, we show that infection with natural obligate intracellular pathogens is impaired by loss of *pnp-1*, the *C. elegans* ortholog of the vertebrate purine nucleoside phosphorylase (PNP), which is an enzyme involved in salvaging purines. Loss of *pnp-1* leads to altered levels of purine nucleotide precursors and increased expression of Intracellular Pathogen Response genes, which are induced by viral and fungal intracellular pathogens of *C. elegans*. In addition, we find that loss of

pnp-1 increases resistance to extracellular pathogen infection and increases expression of genes involved in extracellular pathogen defense. Interestingly, studies from 1975 found that mutations in human PNP impair T-cell immunity, whereas our findings here indicate *C. elegans pnp-1* regulates intestinal epithelial immunity. Overall, our work indicates that host purine homeostasis regulates resistance to both intracellular and extracellular pathogen infection.

Introduction

Obligate intracellular pathogens are completely dependent on their hosts for replication. In most cases, these pathogens lack biosynthetic pathways and thus rely on host cells to obtain building blocks for growth, including nucleotides, amino acids and lipids. In particular, viruses are completely reliant on host nucleotides for replication and transcription. As such, host restriction factors can serve to limit the pool of nucleotides available to viruses and thus block their growth. For example, the human SAM domain and HD domain-containing protein 1 is a restriction factor for Human Immunodeficiency Virus (HIV), acting to degrade the deoxynucleotides needed for reverse transcription of the HIV genome [1]. Even eukaryotic pathogens such as microsporidia appear to lack nucleotide biosynthetic pathways and instead 'steal' nucleotides from host cells [2, 3]. In particular, microsporidia express cell-surface ATP/GTP transporters, which are believed to import host purine nucleotides to support parasite growth and proliferation [4-6].

Microsporidia comprise a phylum of obligate intracellular pathogens related to fungi, with over 1400 species identified [7]. Microsporidia are extremely prevalent in nature and almost all animals are susceptible to infection by at least one microsporidia species [8, 9]. Recent work indicates that these fungal pathogens are the most common cause of infection in the wild for the model nematode *C. elegans* and other related nematodes [10, 11]. The microsporidian *Nematocida parisii* is the pathogen species most often found to infect wild *C. elegans*, and this pathogen goes through its entire replicative life cycle inside the intestine [10]. Interestingly, the host transcriptional response to *N. parisii* appears to be almost identical to the host response to the Orsay virus, which is a 3-gene positive-sense RNA virus and another natural intracellular pathogen of the *C.*

elegans intestine [10, 12-14]. This common transcriptional response has been named the Intracellular Pathogen Response, or IPR, and it appears to constitute a novel defense pathway in *C. elegans* [15]. Although the host sensor for *N. parisii* is not known, we have recently discovered that *drh-1*, a *C. elegans* homolog of the mammalian RIG-I dsRNA sensor, mediates induction of the IPR likely through detecting dsRNA or other RNA replication products of the Orsay virus [16].

Forward genetic studies identified *pals-22* and *pals-25* as antagonistic paralogs that regulate the IPR and associated phenotypes [15, 17]. *pals-22* and *pals-25* belong to the *pals* gene family in *C. elegans*, which contains at least 39 *pals* genes named for the loosely conserved ALS2CR12 protein signature located in the single ALS2CR12 gene found in each of the human and mouse genomes [15, 18, 19]. The biochemical functions of ALS2CR12 and *C. elegans pals* genes are unknown, but *pals-22* and *pals-25* appear to dramatically rewire *C. elegans* physiology. *pals-22* mutants have constitutive expression of IPR genes in the absence of infection, and have improved tolerance of proteotoxic stress, as well as increased resistance against *N. parisii* and the Orsay virus, but decreased resistance against the bacterial extracellular pathogen *Pseudomonas aeruginosa* [15, 17]. A mutation in *pals-25* reverses these phenotypes found in *pals-22* mutants, as *pals-22 pals-25* double mutants have phenotypes similar to wild-type animals, including wild-type levels of IPR gene expression. There are approximately 100 IPR genes, which include other *pals* genes like *pals-5* (although notably not *pals-22* and *pals-25*), as well as components of a cullin RING ubiquitin ligase complex, which is required for the increased tolerance of proteotoxic stress observed in *pals-22* mutants [17, 20].

To gain insight into how *C. elegans* regulate IPR gene expression and related phenotypes, we sought to identify additional regulators of the IPR. Here, we report that *C. elegans pnp-1* is a novel repressor of the IPR. *pnp-1* is the *C. elegans* ortholog of the vertebrate purine nucleoside phosphorylase (PNP), which functions in the purine salvage pathway to regulate levels of purine nucleotides. Interestingly, mutations in human PNP lead to severe combined immunodeficiency disease due to T-cell

dysfunction [21-23]. Our results indicate that, like vertebrate PNP, *C. elegans pnp-1* functions as a purine nucleoside phosphorylase, regulating levels of purine metabolites. We find that *pnp-1* mutants, similar to *pals-22* mutants, display resistance to various natural intestinal pathogens. Surprisingly, unlike *pals-22*, *pnp-1* also negatively regulates the expression of genes that are induced by bacterial infection and by other immune regulators. Moreover, *pnp-1* mutants display resistance to the extracellular bacterial pathogen *P. aeruginosa*. Epistasis analysis indicates that the p38 MAP kinase *pmk-1* is required for the increased resistance of *pnp-1* mutants against extracellular pathogens, but *pmk-1* is not required for the increased resistance of *pnp-1* mutants against intracellular pathogens. In summary, our work indicates that *pnp-1* is a new regulator of the response to both intracellular and extracellular infection, suggesting that purine metabolite levels are important regulators of the response to pathogen infection.

Results

pnp-1 is a negative regulator of IPR gene expression.

To identify negative regulators of the IPR, we performed a forward mutagenesis screen using the established *pals-5p::GFP* transcriptional reporter, which induces GFP expression in the intestine upon *N. parisii* or Orsay virus infection. From this screen, we isolated mutants with constitutive *pals-5p::GFP* expression including the allele *jy90*. After back-crossing *jy90* mutants and mapping the mutation to Chromosome IV, we performed whole genome sequencing to identify the causative allele. From this analysis, we identified a missense mutation in the PNP gene *pnp-1*, which should result in substitution of a conserved serine (S51 or S68 in isoform a or b, respectively) to leucine (Fig 1A). This serine is conserved across phylogeny and has been shown to be required for enzymatic activity of human PNP (S1 Fig 1) [24]. To confirm that a mutation in *pnp-1* can induce *pals-5p::GFP* expression, we used CRISPR/Cas9 editing to generate a deletion allele of *pnp-1* called *jy121*. We found that *pnp-1(jy121)* mutants have constitutive *pals-5p::GFP* expression similar to *pnp-1(jy90)* mutants, confirming that *pnp-1* regulates expression of *pals-5p::GFP* (Fig 1B-1D). In order to test if *pnp-1* regulates expression of endogenous *pals-5* mRNA and not just the *pals-5p::GFP* transgene, we performed qRT-PCR and analyzed the mRNA expression of *pals-5* and

other IPR genes. Here, we found that *pnp-1* mutants constitutively express endogenous mRNA for *pals-5* and other IPR genes in the absence of any IPR trigger (Fig 1E), indicating that wild-type *pnp-1* negatively regulates the mRNA expression of several IPR genes.

pnp-1 mutants have altered levels of purine metabolites

Vertebrate PNP functions in the purine salvage pathway where purine nucleotides sequentially are degraded to nucleosides and purine bases. These bases are then converted back into purine nucleotides. Specifically, PNP converts the nucleosides inosine or guanosine into the bases hypoxanthine or guanine, respectively (S2A Fig). If *pnp-1* were functioning in *C. elegans* as a PNP, *pnp-1* mutants should have higher levels of nucleosides, and lower levels of purine bases. To determine whether this is the case, we performed targeted Liquid Chromatography-Mass Spectrometry metabolomic analysis to quantify these metabolites in *pnp-1* mutants. Indeed, this analysis revealed that *pnp-1* mutants have significantly higher levels of inosine and significantly lower levels of hypoxanthine as compared to wild-type animals (Fig 1F). However, guanine and guanosine were below detectable levels in both mutants and wild-type animals, so comparisons could not be made for these metabolites. No significant changes were found in the levels of any other detected metabolites of the purine salvage pathway or metabolites of the *de novo* purine synthesis pathway in *pnp-1* mutants (S2 Fig). Of note, the levels of inosine and hypoxanthine in *pals-22* mutants were not significantly different than those of wild-type animals, indicating that not all mutants with constitutive IPR gene expression have altered inosine and hypoxanthine levels. In summary, these findings indicate that, similar to its vertebrate ortholog, *C. elegans pnp-1* functions as a PNP to convert purine nucleosides into free purine bases.

pnp-1 mutants have increased resistance to intracellular pathogen infection

As *pnp-1* mutants have constitutive expression of IPR genes, we hypothesized that these mutants should be resistant to intracellular pathogen infection. Therefore, we assessed the pathogen load of Orsay virus and *N. parisii* in *pnp-1* mutants. Here we found that Orsay viral load, as determined by qRT-PCR for the viral genome segment

RNA1, is significantly lower in *pnp-1* mutants as compared to wild-type animals (Fig 2A). We next analyzed *N. parisii* pathogen load at 3 hours post infection (hpi) by counting individual sporoplasms, which are individual parasite cells likely to represent individual invasion events into intestinal cells [25]. We found that *pnp-1* mutants display a significant reduction of the number of sporoplasms per animal as compared to wild-type animals (Fig 2B). We also investigated *N. parisii* pathogen load at 30 hpi, when sporoplasms have developed into replicative meronts within the intestine. At 30 hpi as well, we found that *N. parisii* pathogen load of *pnp-1* mutants is significantly lower than that of wild-type animals (Fig 2C). Of note, *pals-22* mutants have significantly higher resistance to infection than *pnp-1* mutants in these assays (Fig 2A-C).

Consistent with *pnp-1* mutants having lower *N. parsii* pathogen load compared to wild-type animals, we also found that they have increased survival upon infection compared to wild-type animals (Fig 2D, S3 Fig). To address the concern that the pathogen resistance of *pnp-1* mutants is due to feeding defects that lower the exposure of these animals to intestinal pathogens, we fed them fluorescent beads and quantified accumulation in the intestinal lumen. We found that accumulation of these beads is not significantly different in either of the *pnp-1* mutants as compared to wild-type animals, whereas the known feeding-defective *eat-2* mutants displayed significantly less bead accumulation compared to wild-type animals (Fig 2E). Taken together, these results indicate that wild-type *pnp-1* functions to negatively regulate resistance to and survival upon intracellular pathogen infection.

***pnp-1* functions in the intestine to regulate the IPR**

To determine the site of action for *pnp-1*-mediated regulation of the IPR, we investigated its tissue expression using a “TransgeneOme” construct containing PNP-1 tagged at the C terminus with GFP and 3×FLAG, surrounded by a ~20-kb endogenous genomic regulatory region [26]. We generated transgenic animals containing this construct and observed GFP expression in the 20 epithelial cells that comprise the intestine, as well as in several head neurons (Fig 3A, S4 Fig). Importantly, expression of this PNP-1::GFP transgene rescued the decreased number of sporoplasms in *pnp-1*

mutants (Fig 3B), supporting the model that expression from this transgene reflects endogenous PNP-1 expression.

Next, we used single-copy tissue-specific expression to investigate where *pnp-1* regulates IPR phenotypes. In a *pnp-1* mutant background, we generated single copy insertions of *pnp-1* under the control of an intestine-specific promoter (*vha-6*) or a neuron-specific promoter (*unc-119*) into the same genomic locus. Expression of *pnp-1* in the intestine, but not in neurons, rescued the *pnp-1* mutant phenotypes of decreased number of sporoplasms (Fig 3C) and increased expression of IPR genes (Fig 3D). Altogether, these results demonstrate that *pnp-1* acts in intestinal epithelial cells to regulate IPR gene expression and pathogen resistance.

pnp-1 mutants display phenotypes not previously associated with IPR activation

As *pnp-1* had not been characterized before in *C. elegans*, we next explored additional phenotypes. We focused on phenotypes found in *pals-22* mutants, as these mutants have constitutive IPR expression, like *pnp-1* mutants [15, 17]. First, we determined the lifespan of *pnp-1* mutants. In contrast to the short-lived *pals-22* mutants, we found that the lifespan of *pnp-1* mutants appears similar to wild-type animals (Fig 4A, S5 Fig). Second, we investigated the thermotolerance of *pnp-1* mutants, because *pals-22* mutants display increased resistance to proteotoxic stress, including better thermotolerance compared to wild-type animals. Here, *pnp-1* mutants also had a distinct phenotype from *pals-22* mutants, as they displayed significantly decreased thermotolerance as compared to wild-type animals (Figure 4B). Interestingly, *pnp-1* appears to be acting downstream or in parallel of *pals-22* for thermotolerance, as the *pals-22*;*pnp-1* double mutants show decreased thermotolerance, similar to *pnp-1* single mutants (Fig 4C).

We further explored the pathogen resistance phenotypes of *pnp-1* mutants in comparison to *pals-22* mutants. Previous work had shown that *pals-22* mutants have increased susceptibility to the extracellular Gram-negative pathogen *P. aeruginosa* strain PA14 [15]. In contrast to *pals-22* mutants, we found that *pnp-1* mutants are

slightly but significantly resistant to PA14 infection as compared to wild-type animals (Fig 4D). Because the NSY-1/SEK-1/PMK-1 p38 MAP kinase pathway is one of the most important pathways for defense against *P. aeruginosa* in *C. elegans* [27-29], we next investigated whether *pmk-1* was required for this increased resistance of *pnp-1* mutants (Fig 4E). Here we found that *pnp-1 pmk-1* double mutants had PA14 pathogen load more similar to that of *pmk-1* single mutants, indicating that *pmk-1* is required for the enhanced resistance and likely acts downstream or in parallel to *pnp-1*. Loss of *pmk-1* in a *pals-22* mutant background further enhanced susceptibility in this background as well, suggesting that here too, *pmk-1* acts downstream of, or in parallel to, this IPR regulator with respect to extracellular pathogen resistance.

During initial species description and characterization of *N. parisii*, we found very little role for *pmk-1* in resistance to *N. parisii* infection, as assessed by survival upon infection, and by meront and spore load quantified by Nomarski optics [10]. To analyze pathogen resistance in greater detail, here we use the more recently developed method as described above to analyze *pmk-1* resistance at 3 hpi by counting sporoplasms. From this analysis we found that *pmk-1* mutants do have significantly enhanced susceptibility to *N. parisii* infection. Interestingly, this enhanced susceptibility can be suppressed by mutations in *pnp-1* or *pals-22* (Fig 4F), indicating that in contrast to the results with *P. aeruginosa*, *pmk-1* appears to act upstream or in parallel to *pnp-1* and *pals-22* for resistance to *N. parisii*. As there is no significant overlap between IPR genes and those regulated by *pmk-1* [13, 17], *pmk-1* likely functions in parallel to *pnp-1* and *pals-22* in this infection context. These results indicate that the genetic interactions between *pmk-1* and the negative IPR regulators *pnp-1* and *pals-22* depend on the pathogen being tested.

Overall, these results demonstrate that while *pnp-1* and *pals-22* are both negative regulators of IPR gene expression and intracellular pathogen resistance, they have distinct phenotypes with respect to thermotolerance, lifespan and extracellular pathogen resistance.

***pnp-1* mutants have increased expression of most IPR genes**

Next, we sought to determine the full transcriptome changes in *pnp-1* mutants. Therefore, we performed RNA-seq analysis on both *pnp-1* mutants as well as wild-type animals. By differential gene expression analysis (S3 Table), we determined that 286 and 244 genes are upregulated ($p<0.05$, no fold change cut off) in *pnp-1(jy90)* and *pnp-1(jy121)* mutants respectively, compared to wild-type animals. We found that 226 upregulated genes are common to both mutants and that this overlap is statistically significant (Fig 5A). In addition, we compared the genes upregulated in *pnp-1* and *pals-22* mutants and found a significant overlap between these gene sets (Fig 5B). Notably, of the 25 *pals* genes upregulated by *N. parisii* infection and Orsay virus, 22 are significantly up-regulated in both *pnp-1* mutant alleles (Fig 5C). In addition, several other genes that had previously been shown to be upregulated in the IPR are also upregulated in *pnp-1* mutants (Fig 5D).

To more globally evaluate the similarity between genes regulated by *pnp-1* and genes regulated by previously described IPR regulators, we performed Gene Set Enrichment Analysis (GSEA) (S4 and S5 Table) [30], confirming similarity using hypergeometric testing (S6 Table). We determined that *pnp-1* significantly regulates genes that are upregulated by almost all known IPR triggers, including *N. parisii* infection, Orsay virus infection and treatment with the proteasome inhibitor bortezomib (Fig 5E). [Of note, *pnp-1* does not regulate the chitinase-like *chil* genes, which are induced by infection with the oomycete *Myzocytiopsis humicola,* a pathogen that can induce some, but not all IPR genes [17, 31].] Moreover, *pnp-1* regulates genes that are also induced by ectopic expression of the RNA1 segment of Orsay virus that contains an active form of RNA-dependent RNA polymerase. These induced genes include many IPR genes [16].

***pnp-1* negatively regulates genes involved in immunity to extracellular pathogens**

Gene Ontology (GO) term analysis on the genes upregulated in *pnp-1* mutants showed statistically significant enrichment of genes involved in innate immune response (GO:0045087), carbohydrate binding (GO:0030246), defense response to Gram-negative bacteria (GO:0050829) and defense to Gram-positive bacteria (GO:0050830)

(S7 Table) [32]. These GO terms were not previously found to be enriched in genes upregulated by *N. parisii* infection [13]. In addition, we performed a similar analysis with the Wormcat program that identifies significantly over-represented genes in a differentially expressed gene set and bins them into more refined categories than GO terms (Fig 5F, S8 Table) [33]. Wormcat analysis of *pnp-1* upregulated genes shows over-representation of genes involved in pathogen/stress response and proteasome proteolysis, which include genes that encode for proteins containing C-type lectin, CUB and F-box domains. Some of these genes, such as *skr-3, fbxa-158* and *fxba-75* are also upregulated in *pals-22* mutants [17]. However, many non-IPR genes that are induced by bacterial infection, such as *irg-4*, *lys-1* and *dod-23*, are upregulated in *pnp-1* mutants, but not in *pals-22* mutants [28]. This distinction may explain the contrast in resistance to bacterial pathogens between *pnp-1* and *pals-22* mutants.

As *pnp-1* mutants display resistance to PA14 and express various genes involved in bacterial defense, we used GSEA analysis and hypergeometric testing to determine the similarity between genes regulated by *pnp-1* and those regulated in response to infection by various bacterial pathogens (Fig 5G, S4-S6 Tables). We determined that genes upregulated in *pnp-1* mutants are significantly similar to those induced by the Gram-negative pathogens *P. aeruginosa* and *Serratia marcescens*. In addition, we used GSEA analysis to investigate the similarity between gene regulated by *pnp-1* and those regulated by known immune regulators. We determined that genes regulated by *pnp-1* are significantly similar to those regulated by the transcription factors *sta-1*, *skn-1*, *hsf-1*, as well as *pmk-1* and its upstream MAP Kinase Kinase *sek-1*. Previous GSEA analysis of genes up-regulated in *pals-22* mutants and by *N. parisii* infection showed very little similarity to genes induced by these extracellular pathogens and immune regulators. Taken together, these gene expression analyses indicate that, in addition to regulating the IPR, *pnp-1* may play a broader role in regulating *C. elegans* immunity to bacterial pathogens.

Discussion

Here, we describe a role for purine metabolism in regulating intestinal epithelial cell defense against pathogen infection in the nematode *C. elegans* (Fig 6). Purine metabolism pathways are conserved from prokaryotes to humans and include the energy-expensive de novo synthesis pathway and the less energy-costly salvage pathway that recycles nucleotides (S2A Fig) [34]. While recent reports have implicated purine metabolism in *C. elegans* longevity and development, specific characterization of the salvage pathway has not previously been reported [35, 36]. Through a forward genetic screen, we identified the salvage enzyme *pnp-1* as a negative regulator of the IPR, a common transcriptional response to intracellular pathogens. Our analysis of *pnp-1* represents the first characterization of purine nucleoside phosphorylase and, more broadly, the purine salvage pathway in *C. elegans.* We found that *pnp-1* mutants are resistant to the natural intracellular pathogens *N. parisii* and the Orsay virus (Fig 2). This resistance phenotype is in common with *pals-22* mutants, which also have upregulated IPR gene expression [17]. While much remains to be defined about the regulation and outputs of IPR genes, these findings are consistent with the model that upregulation of IPR genes promotes defense against intracellular pathogens.

IPR gene upregulation in *pals-22* mutants has been associated with several other phenotypes, including increased proteostasis characterized by increased thermotolerance [15]. This increased thermotolerance of *pals-22* mutants is completely dependent on IPR genes that encode components of a multi-subunit cullin ring ubiquitin ligase complex, including the cullin *cul-6* and the F-box proteins *fbxa-75* and *fbxa-158* [20]. These IPR genes are also upregulated in *pnp-1* mutants, but surprisingly *pnp-1* mutants have greatly decreased thermotolerance compared to wild-type animals (Fig 4). One potential explanation for this distinction is that *pnp-1* mutants may have less metabolic flexibility upon heat shock than wild-type animals. *pnp-1* mutants are defective in the purine salvage pathway, which is less energy-costly than the de novo synthesis pathway. Under normal conditions the salvage pathway is preferentially used, but in response to high purine demands such as heat shock, the de novo pathway is activated to increase purine metabolic flux [37-43]. One possibility is that *pnp-1* mutants have constitutive use of the de novo pathway, and so are unable to increase purine

metabolic flux upon heat shock, resulting in decreased thermotolerance. The observation that the *pnp-1* thermotolerance phenotype is epistatic to *pals-22* is consistent with this model, as there should be a requirement for appropriate purine metabolic flux upon heat shock, regardless of genetic background.

Another phenotype that is distinct between *pnp-1* and *pals-22* mutants is resistance to *P. aeruginosa*, with *pals-22* mutants susceptible and *pnp-1* mutants resistant to this extracellular bacterial pathogen (Fig 4). Transcriptomic analysis provided a likely explanation for this discrepancy, as *pnp-1* mutants have upregulated expression of many genes that are induced by bacterial infection and by previously described immunity pathways including the PMK-1 p38 MAPK pathway, whereas *pals-22* mutants do not. Consistent with the model that resistance of *pnp-1* mutants depends on *pmk-1*-induced genes, we find that *pmk-1* was required for the increased resistance of *pnp-1* mutants to *P. aeruginosa*. However, it should be noted that *pmk-1* mutations can suppress the resistance phenotypes of other mutants, such as *daf-2* mutants, which have very few *pmk-1* genes upregulated [28]. Therefore, the requirement for *pmk-1* in the resistance of *pnp-1* mutants may be unrelated to their regulation of similar genes, although that is an attractive model (Fig 6).

How does constitutive upregulation of IPR genes in both *pnp-1* and *pals-22* mutants lead to increased resistance to intracellular pathogens at early timepoints? The ubiquitin ligase components mentioned above appear to play a minor role in pathogen resistance [13, 20], indicating that there is either extensive redundancy in these components, other IPR genes are more important, or there may be a non-transcriptional component that enables resistance in these mutants. Given that the *N. parisii* parasite cells at 3 hpi are likely the result of initial invasion events, perhaps some host factor regulating intestinal cell invasion is altered in these mutants. Further analysis of individual IPR genes may yield insight into the mechanism of resistance against *N. parisii* in these mutants.

Which purine metabolites regulate the expression of IPR and other pathogen response genes in *pnp-1* mutants? Our metabolomics analysis confirmed that, as predicted, *pnp-*

372 *1* mutants have increased levels of inosine, the nucleoside substrate for *pnp-1*, and
373 decreased levels of hypoxanthine, the purine base product of *pnp-1* (Fig 1). No other
374 metabolites were found to have altered levels in these mutants (S2 Fig). Therefore,
375 inosine may be an activator, or hypoxanthine a repressor, of pathogen response gene
376 expression. However, it is possible that altered levels of some other unknown
377 metabolites in *pnp-1* mutants are regulators of the IPR, or perhaps *pnp-1* regulates the
378 IPR in a manner independent of its enzymatic activity. Support for the model that the
379 catalytic activity of *pnp-1* is required for its effects on the IPR comes from the *pnp-*
380 *1*(*jy90*) allele, which has a conserved serine mutated to leucine. When this residue is
381 mutated in the human ortholog it leads to an inactive enzyme, suggesting that *pnp-1*
382 enzymatic function is key to its regulation of the IPR [24].
383
384 All life, including eukaryotes, prokaryotes and viruses, require purines as part of
385 deoxynucleotides for DNA and ribonucleotides for RNA. Obligate intracellular pathogens
386 as diverse as viruses and the eukaryotic pathogens *Plasmodium falciparum* and
387 microsporidia depend on their hosts for purines, with several types of transporters
388 identified in eukaryotic pathogens used to steal purines from hosts [4-6, 44-46].
389 Extensive work on purine metabolism and its effects on human physiology have come
390 from studies of so-called 'inborn errors of metabolism', which are often due to mutations
391 in purine enzymes [21, 38, 47-50]. Interestingly, although mutations in enzymes of the
392 purine de novo and salvage pathways cause of various disorders (e.g. deafness,
393 intellectual disability, motor dysfunction, renal failure), only mutations in purine salvage
394 enzymes result in immunodeficiency due to T-cell dysfunction [51, 52]. While the focus
395 is on the detrimental effects of these mutations, it is interesting to speculate that there
396 be some advantage conferred by these mutations in terms of resistance to infection,
397 perhaps in the heterozygote state, or against certain pathogens and/or in certain cell
398 types. While mutations in human PNP cause severe combined immunodeficiency, this
399 phenotype appears to be due to apoptosis of T cells [53, 54]. Less has been described
400 about the role of PNP in intestinal epithelial cells, which is the cell type where *C.*
401 *elegans pnp-1* mutants have increased pathogen resistance. Further work on purine
402 metabolism and how it regulates immunity may help shed light on whether sensing

403 altered levels of purine metabolites may enable hosts to monitor the effects of pathogen
404 infection as part of surveillance immunity to induce epithelial cell defense.
405

406 ## Methods

407 ### *C. elegans* strains

408 All worm strains were maintained by standard methods [55]. Briefly, worms were grown
409 on NGM plates seeded with *E. coli* strain OP50-1 and grown at 20°C. All mutant and
410 transgenic strains were backcrossed a minimum of three times. See S1 Table for a list
411 of strains used. For several experiments, synchronized L1 worms were prepared by
412 bleaching gravid adults to isolate embryos that hatched in M9 buffer into starved,
413 synchronized L1 worms.
414

415 **Forward mutagenesis screening and cloning of *pnp-1(jy90)***

416 Ethyl methane sulfonate (EMS) (Sigma) mutagenesis of *jyIs8* [*pals-5p::GFP*, *myo-*
417 *2p::mCherry*] animals was performed by standard procedures [56]. P0 worms were
418 incubated with 50 mM EMS at 20°C for 4 hours with constant rotation. Using a
419 fluorescence dissecting microscope (Zeiss Discovery V8), mutant F2 animals
420 ectopically expressing *pals-5p::GFP* were isolated. ~26,000 haploid genomes were
421 screened. From this screen, we identified 9 mutant alleles that result in robust ectopic
422 GFP expression. Four mutants failed to complement the constitutive *pals-5p::GFP*
423 expression phenotype of *pals-22* mutants, indicating that they likely have mutations in
424 *pals-22*. The other five alleles complement each other for the *pals-5p::GFP* expression
425 phenotype, indicating that they have mutations in 5 distinct genes. *jy90* was mapped to
426 Linkage Group (LG) IV using visible makers contained in the strains ERT507, ERT508,
427 and ERT509 and confirmed by linkage group mapping using SNP primers [57]. DNA
428 was prepared using Puregene Core kit (QIAGEN) for whole genome sequencing and
429 submitted to Beijing Genomics Institute for sequencing with a 100 bp paired-end
430 Illumina HiSeq 4000 with 30X coverage. Analysis identified one gene (*pnp-1*) on LG IV
431 that harbored a variant predicted to alter gene function. *pnp-1(jy90)* contains a G to A
432 substitution that should convert serine to leucine in isoform A and serine 68 to leucine in
433 isoform B.

434

435 **CRISPR/Cas9-mediated gene deletion of *pnp-1***

436 A co-CRISPR protocol was used to generate a complete deletion of *pnp-1* [58]. Two
437 CRISPR RNAs (crRNA) were designed to target the 5' end
438 (TGATTTCATTGGCTTCCACG) and 3' end (AGTTTTTTCTGTGAACCACG) of the
439 gene. A crRNA against *dpy-10* was used as a control. All three cRNAs and tracrRNA
440 were synthesized by Integrated DNA Technologies (IDT) and resuspended in IDT
441 nuclease-free duplex buffer to 100 µM. An injection mix was made by first annealing 0.5
442 µl of three crRNAs with 2.5 µl tracrRNA, then complexing the annealed sgRNA with
443 purified 3.5 µl of 40 µM Cas9 protein. This mix was injected into the gonads of *jyIs8*
444 worms. Dumpy (Dpy) and/or GFP-positive F1 animals were selected and genotyped for
445 deletions of the *pnp-1* locus. After submitting to Sanger sequencing to confirm the
446 presence of a complete deletion, one strain was selected and named allele *jy121*. *jy121*
447 was backcrossed to *jyIs8* three times and then outcrossed to N2.

448

449 **Generation of transgenic strains**

450 For the transgenic expression reporter of *PNP-1* protein:
451 The *pnp-1* TransgeneOme fosmid
452 (K02D7.1[20219]::S0001_pR6K_Amp_2xTY1ce_EGFP_FRT_rpsl_neo_FRT_3xFlag)dF
453 RT::unc-119-Nat) was injected into EG6699 at 100 ng/µl to generate strain ERT879.

454

455 For fosmid rescue of the *pnp-1(jy90)* mutant phenotype:
456 The following injection mix was made and injected into *pnp-1(jy90)* mutants to generate
457 strain ERT869*: myo-2p*::*mCherry* (10 ng/µl)*, pnp-1* transgeneOme fosmid (25 ng/µl),
458 genomic N2 DNA (65 ng/µl).

459

460 For single-copy tissue-specific *pnp-1* rescue strains:
461 CRISPR/Cas9 genome editing was used to insert tissue-specific expression cassettes
462 at cxTi10882 on Chromosome IV as previously described, in a so-called "Cas-SCI
463 (Single-Copy Insertion) technique" [59]. Briefly, we generated plasmids pET721 (*vha-*
464 *6::pnp-1*::3XFLAG::GFP::*unc-54*) and pET720 (*unc-119::pnp-1*::3XFLAG::*unc-54*) by

assembling the tissue-specific cassettes (including *unc-54* 3' UTR) into plasmid pCZGY2729 such that the tissue-specific cassettes and the hygromycin resistance gene were flanked by homology arms to cxTi10882. These plasmids (25 ng/µl) were then injected into N2 animals along with pCZGY2750 that expresses Cas9 and sgRNA for cxTi10882. pCFJ10 *myo-3p::mCherry* (5 ng/µl) and pCFJ90 *myo-2p*::*mCherry* (2 ng/µl) were used a co-injection markers. Genomic insertion was determined by identifying animals resistant to hygromycin that did not express the co-injection markers. Single-copy insertion lines were verified by genotyping.

RNA extraction and qRT-PCR

RNA was extracted using TRI reagent and 1-Bromo-3-chloropropane (Molecular Research Center, Inc.), according to the manufacturer's instructions, and converted to cDNA using the iScript (Bio-Rad) cDNA synthesis kit. qRT-PCR was performed using iQ SYBR green supermix (Bio-Rad) and various gene specific primers (S1 Table) on a BioRad CFX Connect real-time system. Each biological replicate was performed in duplicate and normalized to *nhr-23 or snb-1*, control genes that did not change expression in these experiments. Three experimental replicates were performed.

Thermotolerance Assays

Gravid adults were picked to NGM plates and grown at 20^{o}C. L4 progeny from these adults were picked to fresh NGM plates and submitted to a heat shock of 37^{o}C for two hours. Animals were allowed to recover for 30 minutes at room temperature, then incubated at 20^{o}C for 24 hours, and then scored for survival. During both the heat shock and recovery, plates were placed in a single layer (plates were not stacked on top of each other). Worms were defined as dead by lack of movement on the plate, lack of pharyngeal pumping and lack of response to touch. For each replicate, three plates containing 30 worms were scored per genotype. Three experimental replicates were performed.

Targeted Metabolomics

Synchronized L1 worms were plated on NGM plates seeded with OP50-1 and grown to Day 1 adult stage at 20^{o}C. Fifteen 6 cm plates were used for each genotype per experiment and 6 experiments were performed. Metabolite extraction and LC-MS were performed with the Penn State Metabolomics Core facility as previously described [60]. Raw Data were processed with MS-DIAL and metabolite levels were corrected to chlorpropamide, an internal standard. Selected metabolites were identified by m/z and column retention time values of known standards. Normalized area under the curve for each metabolite is represented as arbitrary units in graphs.

N. parisii infection

N. parisii spores were isolated as previously described [25]. 1200 synchronized L1 worms were mixed with 5x10^{6} *N. parisii* spores, 25 µl 10X concentrated OP50-1 bacteria and M9 to bring the total volume to 300 µl. This mixture was then plated on room temperature unseeded 6 cm NGM plates, allowed to dry and then incubated at 25^{o}C for 3 or 30 hours. Three plates were used per genotype. Animals were fixed in 4% paraformaldehyde and then stained using a FISH probe specific to *N. parisii* ribosomal RNA conjugated to Cal Fluor 610 dye (Biosearch Technologies). For the 3 hpi timepoint, pathogen load was determined by counting sporoplasms per worms using 40x objective on a Zeiss AxioImager M1 microscope. For each replicate, 75 animals per genotype were quantified. Three experimental replicates were performed. For the 30 hpi timepoint, pathogen load was quantified using the COPAS Biosort machine (Union Biometrica). The *N. parisii* FISH signal for each worm was normalized to the length of the worm using time-of-flight measurements. For each replicate, 100 animals per genotype were quantified.

Bead Feeding assay

1200 synchronized L1 worms were mixed with 6 µl fluorescent beads (Fluoresbrite Polychromatic Red Microspheres, Polysciences Inc.). 25 µl 10X concentrated OP50-1 bacteria and M9 to bring the total volume to 300 ul. This mixture was then plated on room temperature unseeded 6 cm plates, allowed to dry and then incubated at 25^{o}C for 5 mins. Plates were immediately shifted to ice, washed with ice cold PBS-Tween and

fixed in 4% paraformaldehyde. Worms were imaged with the 4x objective on an ImageXpress Nano plate reader. Using FIJI software, the integrated density of bead fluorescence per worm was quantified from which background fluorescence was subtracted giving the Corrected Total Fluorescence (CTF) for each worm. For each replicate, 50 animals per genotype were quantified. Three experimental replicates were performed.

P. aeruginosa infection

Slow Killing (SK) plates with 50 µg/ml ampicillin were seeded with overnight cultures of PA14-dsRED [61], and then incubated at 37^{o}C for 24 hours followed by a 24 hour incubation at 25^{o}C. 3000 synchronized L1 worms were plated onto NGM plates seeded with OP50 and allowed to grow to L4 at 20^{o}C. L4 worms were washed with M9, transferred to the PA14 dsRED SK plates and incubated at 25^{o}C for 16 hours. Worms were then washed with M9 and PA14-dsRED fluorescence per animal was quantified using the COPAS Biosort machine (Union Biometrica). For each replicate, 100 animals per genotype were quantified. Three experimental replicates were performed.

Orsay virus infection

Orsay virus filtrates were prepared as previously described [13]. To prepare worms for infection, ~2,000 synchronized L1 worms were plated onto five 10 cm NGM plates containing a lawn of OP50-1. Plates were incubated at 20°C for 2 days until the L4 stage. To prepare viral plates, 10 µl of the Orsay virus filtrate was mixed with 300 µl of a 10X concentration of OP50-1 and 190 µl M9 buffer, and then this mixture was plated onto 6-cm NGM plates and dried at room temperature. The L4 worms were washed off the 10 cm NGM plates and 500 worms were added to each of the Orsay containing plates and incubated at 20°C for 24 h. RNA was extracted isolated using Tri-reagent (Molecular Research Center, Inc and converted to cDNA with iScript (Bio-Rad) cDNA synthesis kit. qRT-PCR was performed using iQ SYBR green supermix (Bio-Rad) and primers specific to RNA1 of Orsay virus. All gene expression was normalized to *snb-1* expression, which does not change upon conditions tested. Four experimental replicates were performed.

557

558 **Survival and Lifespan Assays**

559 For lifespan assays, ~50 synchronized L1 worms/plate per strain were plated onto six
560 3.5 cm tissue culture-treated NGM plates seeded with OP50-1. Plates were incubated
561 at 25°C. After 66 hours, 30 adults per strain were scored in triplicate and live animals
562 were transferred to fresh plates. Plates were incubated at 25°C and live worms were
563 transferred every 24 h until death or until progeny production stopped. Survival was
564 measured every 24 h and worms that did not respond to touch were scored as dead.
565 Animals that died from internal hatching or crawled off the plate were censored. Three
566 experimental replicates were performed. Survival assays were performed in the same
567 manner as lifespan assays with the addition of an initial *N. parisii* infection. For infection,
568 ~100 synchronized L1 worms were plated with a mixture of 50 µl of a 10X concentration
569 of OP50-1 *E. coli* and 5 x 10^4 *N. parisii* spores onto a 3.5 cm tissue culture-treated NGM
570 plate. Number of spores added was determined by finding the dosage that resulted in
571 approximately 50% killing rate in wild-type worms after 100 hours. Four experimental
572 replicates were performed.

573

574 **RNA-seq sample preparation and sequencing**

575 ~3,000 synchronized L1 worms/plate per strain were plated onto a 10 cm NGM plate
576 seeded with OP50-1 and allowed to grow for 56 hours at 20°C. As *pnp-1* mutants grow
577 slightly slower, wild-type L1 worms were plated 1 hour after *pnp-1(jy90)* and *pnp-*
578 *1(jy121)* so they were synchronized in age at harvest time. RNA was extracted using
579 TRI reagent and BCP (Molecular Research Center, Inc.) according to the
580 manufacturer's instructions and additionally purified using the RNeasy cleanup kit with
581 gDNA Eliminator spin columns (Qiagen). RNA quality was assessed using a
582 TapeStation system. Sequencing libraries were constructed using TruSeq stranded
583 mRNA method and sequenced using run type PE100 on an Illumina NovaSeq6000
584 sequencer (Illumina). RNA quality assessment and RNA-seq were conducted at the
585 IGM Genomics Center, University of California, San Diego, La Jolla, CA.

586

587 **RNA-seq and Functional Expression analysis**

In Rstudio, sequencing reads for *pnp-1(jy90)*, *pnp-1(jy121)* and N2 were aligned to the Wormbase WS235 release using Rsubreads and quantified using Featurecounts. Using the Galaxy web platform and the public server at usegalaxy.org, differential gene expression analysis was performed using limma-voom in which undetected and lowly expressed genes (CPM of less than one) were filtered out. An adjusted p-value of 0.05 and no fold-change cutoff was used to define differentially expressed genes. This gene set was used for GO term enrichment analysis (Galaxy) [62] and Wormcat analysis (wormcat.com) [33].

Gene Set Enrichment Analysis v3.0 software was used for functional analysis [30]. Normalized RNA-sequence expression data was converted into a GSEA compatible filetype and used for analysis. The gene sets for comparison were made in Excel and then converted into a GSEA compatible file type. Independent GSEA analysis was performed for *pnp-1(jy90)* vs N2 and *pnp-1(jy121)* vs N2 gene sets. For both analyses, a signal-to-noise metric with 1000 permutations was used. Heatmaps for the NES results were made using Morpheus (https://software.broadinstitute.org/morpheus/). Gene sets that showed significant similarity to *pnp-1(jy90)* and *pnp-1(jy121)* differentially expressed genes were submitted to a hypergeometric test (nemates.org). Representation factors and their p-values for the overlap of *pnp-1(jy90*) or *pnp-1(jy121)* and individual gene sets were calculated using the size of the RNA-seq data set after filtering [11539 for *pnp-1(jy90)* and 11537 for *pnp-1(jy121*)].

Statistics

For all data:

Statistical analysis was performed in Prism 8. Means with error bars as standard deviation are presented unless otherwise noted. For sporoplasm experiments, the box represents the 50% of the data closest to the median and the whiskers span the values outside the box. For metabolite experiments, error bars represent the standard error of the means. Statistical significance indicated as follows: ns indicates not significant, * indicates $p < 0.05$, ** indicates $p < 0.01$, *** indicates $p < 0.001$, **** indicates $p < 0.0001$

For lifespan and survival assays:
The survival of each mutant population was compared to that of the wild-type population in Prism 8 with the Log-rank (Mantel-Cox) test. A *p*-value <0.05 was considered significantly different from control.

For qPCR assays:
Unpaired, one-tailed student t-test was used.

For all pathogen load and thermotolerance assays:
For comparisons between three or more genotypes, means of pathogen loads for three biological replicates were compared using One-way ANOVA test with the Bonferroni correction. For comparisons between two genotypes, means of pathogen loads for three biological replicates were compared using a two-tailed t-test. A *p*-value < 0.05 was considered significantly different.

For RNA-seq and Functional Expression analysis:
For GSEA, a *p*-value < 0.05 or FDR < 0.25 was considered significantly similar. For the hypergeometric test, a *p*-value < 0.05 was considered significantly similar.

Imaging

Worms were anesthetized with 10 mM sodium azide and mounted on 2% agarose pads for analysis on a Zeiss Axioimager Z1 compound microscope.

Acknowledgements

We thank Spencer Gang and Vladimir Lazetic for helpful feedback on the manuscript. We thank Jessica Sowa for preparing the viral filtrate, and Yishi Jin and Matt Andrusiak for reagents and help with the CRISPR/Cas9-mediated single-copy insertion “Cas-SCI” technique. This work was supported by NIH under R01 AG052622 and GM114139 to ERT, and by NIGMS/NIH award K12GM068524 to ET. This publication includes data generated at the UC San Diego IGM Genomics Center utilizing an Illumina NovaSeq

6000 that was purchased with funding from a National Institutes of Health SIG grant (#S10 OD026929). Some strains were provided by the CGC, which is funded by NIH Office of Research Infrastructure Programs (P40 OD010440).

References

1. Pan X, Baldauf HM, Keppler OT, Fackler OT. Restrictions to HIV-1 replication in resting CD4+ T lymphocytes. Cell Res. 2013;23(7):876-85.
2. Dean P, Hirt RP, Embley TM. Microsporidia: Why Make Nucleotides if You Can Steal Them? PLoS Pathog. 2016;12(11):e1005870.
3. Cuomo CA, Desjardins CA, Bakowski MA, Goldberg J, Ma AT, Becnel JJ, et al. Microsporidian genome analysis reveals evolutionary strategies for obligate intracellular growth. Genome Res. 2012;22(12):2478-88.
4. Major P, Sendra KM, Dean P, Williams TA, Watson AK, Thwaites DT, et al. A new family of cell surface located purine transporters in Microsporidia and related fungal endoparasites. Elife. 2019;8.
5. Heinz E, Hacker C, Dean P, Mifsud J, Goldberg AV, Williams TA, et al. Plasma membrane-located purine nucleotide transport proteins are key components for host exploitation by microsporidian intracellular parasites. PLoS Pathog. 2014;10(12):e1004547.
6. Tsaousis AD, Kunji ER, Goldberg AV, Lucocq JM, Hirt RP, Embley TM. A novel route for ATP acquisition by the remnant mitochondria of Encephalitozoon cuniculi. Nature. 2008;453(7194):553-6.
7. Han B, Weiss LM. Microsporidia: Obligate Intracellular Pathogens within the Fungal Kingdom. . Microbiology Spectrum. 2017.
8. Stentiford GD, Becnel J, Weiss LM, Keeling PJ, Didier ES, Williams BP, et al. Microsporidia - Emergent Pathogens in the Global Food Chain. Trends Parasitol. 2016;32(4):336-48.
9. Weber R, Bryan RT, Schwartz DA, Owen RL. Human microsporidial infections. Clin Microbiol Rev. 1994;7(4):426-61.
10. Troemel ER, Felix MA, Whiteman NK, Barriere A, Ausubel FM. Microsporidia are natural intracellular parasites of the nematode Caenorhabditis elegans. PLoS Biol. 2008;6(12):2736-52.
11. Zhang G, Sachse M, Prevost MC, Luallen RJ, Troemel ER, Felix MA. A Large Collection of Novel Nematode-Infecting Microsporidia and Their Diverse Interactions with Caenorhabditis elegans and Other Related Nematodes. PLoS Pathog. 2016;12(12):e1006093.
12. Troemel ER. Host-Microsporidia Interactions in Caenorhabditis elegans, a Model Nematode Host. Microbiol Spectr. 2016;4(5).
13. Bakowski MA, Desjardins CA, Smelkinson MG, Dunbar TL, Lopez-Moyado IF, Rifkin SA, et al. Ubiquitin-mediated response to microsporidia and virus infection in C. elegans. PLoS Pathog. 2014;10(6):e1004200.

14. Felix MA, Ashe A, Piffaretti J, Wu G, Nuez I, Belicard T, et al. Natural and experimental infection of Caenorhabditis nematodes by novel viruses related to nodaviruses. PLoS Biol. 2011;9(1):e1000586.
15. Reddy KC, Dror T, Sowa JN, Panek J, Chen K, Lim ES, et al. An Intracellular Pathogen Response Pathway Promotes Proteostasis in C. elegans. Curr Biol. 2017;27(22):3544-53 e5.
16. Sowa JN, Jiang H, Somasundaram L, Tecle E, Xu G, Wang D, et al. The C. elegans RIG-I homolog DRH-1 mediates the Intracellular Pathogen Response upon viral infection. J Virol. 2019.
17. Reddy KC, Dror T, Underwood RS, Osman GA, Elder CR, Desjardins CA, et al. Antagonistic paralogs control a switch between growth and pathogen resistance in C. elegans. PLoS Pathog. 2019;15(1):e1007528.
18. Leyva-Diaz E, Stefanakis N, Carrera I, Glenwinkel L, Wang G, Driscoll M, et al. Silencing of Repetitive DNA Is Controlled by a Member of an Unusual Caenorhabditis elegans Gene Family. Genetics. 2017;207(2):529-45.
19. Hentati A, Bejaoui K, Pericak-Vance MA, Hentati F, Speer MC, Hung WY, et al. Linkage of recessive familial amyotrophic lateral sclerosis to chromosome 2q33-q35. Nat Genet. 1994;7(3):425-8.
20. Panek J, Gang SS, Reddy KC, Luallen RJ, Fulzele A, Bennett EJ, et al. A cullin-RING ubiquitin ligase promotes thermotolerance as part of the intracellular pathogen response in Caenorhabditis elegans. Proc Natl Acad Sci U S A. 2020;117(14):7950-60.
21. Fox IH. Metabolic basis for disorders of purine nucleotide degradation. Metabolism: clinical and experimental. 1981;30(6):616-34.
22. Fekrvand S, Yazdani R, Abolhassani H, Ghaffari J, Aghamohammadi A. The First Purine Nucleoside Phosphorylase Deficiency Patient Resembling IgA Deficiency and a Review of the Literature. Immunological investigations. 2019;48(4):410-30.
23. Giblett ER, Ammann AJ, Wara DW, Sandman R, Diamond LK. Nucleoside-phosphorylase deficiency in a child with severely defective T-cell immunity and normal B-cell immunity. Lancet. 1975;1(7914):1010-3.
24. Erion MD, Takabayashi K, Smith HB, Kessi J, Wagner S, Honger S, et al. Purine nucleoside phosphorylase. 1. Structure-function studies. Biochemistry. 1997;36(39):11725-34.
25. Balla KM, Andersen EC, Kruglyak L, Troemel ER. A wild C. elegans strain has enhanced epithelial immunity to a natural microsporidian parasite. PLoS Pathog. 2015;11(2):e1004583.
26. Sarov M, Murray JI, Schanze K, Pozniakovski A, Niu W, Angermann K, et al. A genome-scale resource for in vivo tag-based protein function exploration in C. elegans. Cell. 2012;150(4):855-66.
27. Kim DH, Feinbaum R, Alloing G, Emerson FE, Garsin DA, Inoue H, et al. A conserved p38 MAP kinase pathway in Caenorhabditis elegans innate immunity. Science. 2002;297(5581):623-6.
28. Troemel ER, Chu SW, Reinke V, Lee SS, Ausubel FM, Kim DH. p38 MAPK regulates expression of immune response genes and contributes to longevity in C. elegans. PLoS Genet. 2006;2(11):e183.

29. Shivers RP, Pagano DJ, Kooistra T, Richardson CE, Reddy KC, Whitney JK, et al. Phosphorylation of the conserved transcription factor ATF-7 by PMK-1 p38 MAPK regulates innate immunity in Caenorhabditis elegans. PLoS Genet. 2010;6(4):e1000892.
30. Subramanian A, Tamayo P, Mootha VK, Mukherjee S, Ebert BL, Gillette MA, et al. Gene set enrichment analysis: a knowledge-based approach for interpreting genome-wide expression profiles. Proc Natl Acad Sci U S A. 2005;102(43):15545-50.
31. Osman GA, Fasseas MK, Koneru SL, Essmann CL, Kyrou K, Srinivasan MA, et al. Natural Infection of C. elegans by an Oomycete Reveals a New Pathogen-Specific Immune Response. Curr Biol. 2018;28(4):640-8 e5.
32. Huang da W, Sherman BT, Lempicki RA. Bioinformatics enrichment tools: paths toward the comprehensive functional analysis of large gene lists. Nucleic Acids Res. 2009;37(1):1-13.
33. Holdorf AD, Higgins DP, Hart AC, Boag PR, Pazour GJ, Walhout AJM, et al. WormCat: An Online Tool for Annotation and Visualization of Caenorhabditis elegans Genome-Scale Data. Genetics. 2020;214(2):279-94.
34. Chua SM, Fraser JA. Surveying purine biosynthesis across the domains of life unveils promising drug targets in pathogens. Immunology and cell biology. 2020;98(10):819-31.
35. Gao AW, Smith RL, van Weeghel M, Kamble R, Janssens GE, Houtkooper RH. Identification of key pathways and metabolic fingerprints of longevity in C. elegans. Exp Gerontol. 2018;113:128-40.
36. Marsac R, Pinson B, Saint-Marc C, Olmedo M, Artal-Sanz M, Daignan-Fornier B, et al. Purine Homeostasis Is Necessary for Developmental Timing, Germline Maintenance and Muscle Integrity in Caenorhabditis elegans. Genetics. 2019;211(4):1297-313.
37. Becker MA, Losman MJ, Kim M. Mechanisms of accelerated purine nucleotide synthesis in human fibroblasts with superactive phosphoribosylpyrophosphate synthetases. J Biol Chem. 1987;262(12):5596-602.
38. Thompson LF, Willis RC, Stoop JW, Seegmiller JE. Purine metabolism in cultured human fibroblasts derived from patients deficient in hypoxanthine phosphoribosyltransferase, purine nucleoside phosphorylase, or adenosine deaminase. Proc Natl Acad Sci U S A. 1978;75(8):3722-6.
39. An S, Kumar R, Sheets ED, Benkovic SJ. Reversible compartmentalization of de novo purine biosynthetic complexes in living cells. Science. 2008;320(5872):103-6.
40. Zhao H, Chiaro CR, Zhang L, Smith PB, Chan CY, Pedley AM, et al. Quantitative analysis of purine nucleotides indicates that purinosomes increase de novo purine biosynthesis. J Biol Chem. 2015;290(11):6705-13.
41. Chan CY, Zhao H, Pugh RJ, Pedley AM, French J, Jones SA, et al. Purinosome formation as a function of the cell cycle. Proc Natl Acad Sci U S A. 2015;112(5):1368-73.
42. Doigneaux C, Pedley AM, Mistry IN, Papayova M, Benkovic SJ, Tavassoli A. Hypoxia drives the assembly of the multienzyme purinosome complex. J Biol Chem. 2020;295(28):9551-66.

43. Pedley AM, Benkovic SJ. A New View into the Regulation of Purine Metabolism: The Purinosome. Trends Biochem Sci. 2017;42(2):141-54.
44. Downie MJ, Saliba KJ, Howitt SM, Bröer S, Kirk K. Transport of nucleosides across the Plasmodium falciparum parasite plasma membrane has characteristics of PfENT1. Mol Microbiol. 2006;60(3):738-48.
45. El Bissati K, Zufferey R, Witola WH, Carter NS, Ullman B, Ben Mamoun C. The plasma membrane permease PfNT1 is essential for purine salvage in the human malaria parasite Plasmodium falciparum. Proc Natl Acad Sci U S A. 2006;103(24):9286-91.
46. Dean P, Major P, Nakjang S, Hirt RP, Embley TM. Transport proteins of parasitic protists and their role in nutrient salvage. Frontiers in Plant Science. 2014;5(153).
47. Flinn AM, Gennery AR. Adenosine deaminase deficiency: a review. Orphanet J Rare Dis. 2018;13(1):65.
48. Torres RJ, Puig JG. Hypoxanthine-guanine phosophoribosyltransferase (HPRT) deficiency: Lesch-Nyhan syndrome. Orphanet J Rare Dis. 2007;2:48.
49. Kelley RE, Andersson HC. Disorders of purines and pyrimidines. Handbook of clinical neurology. 2014;120:827-38.
50. Tangye SG, Al-Herz W, Bousfiha A, Chatila T, Cunningham-Rundles C, Etzioni A, et al. Human Inborn Errors of Immunity: 2019 Update on the Classification from the International Union of Immunological Societies Expert Committee. J Clin Immunol. 2020;40(1):24-64.
51. Whitmore KV, Gaspar HB. Adenosine Deaminase Deficiency – More Than Just an Immunodeficiency. Frontiers in Immunology. 2016;7(314).
52. Grunebaum E, Cohen A, Roifman CM. Recent advances in understanding and managing adenosine deaminase and purine nucleoside phosphorylase deficiencies. Current opinion in allergy and clinical immunology. 2013;13(6):630-8.
53. Markert ML. Purine nucleoside phosphorylase deficiency. Immunodefic Rev. 1991;3(1):45-81.
54. Papinazath T, Min W, Sujiththa S, Cohen A, Ackerley C, Roifman CM, et al. Effects of purine nucleoside phosphorylase deficiency on thymocyte development. J Allergy Clin Immunol. 2011;128(4):854-63.e1.
55. Brenner S. The genetics of Caenorhabditis elegans. Genetics. 1974;77(1):71-94.
56. Kutscher LM, Shaham S. Forward and reverse mutagenesis in C. elegans. WormBook. 2014:1-26.
57. Davis MW, Hammarlund M, Harrach T, Hullett P, Olsen S, Jorgensen EM. Rapid single nucleotide polymorphism mapping in C. elegans. BMC Genomics. 2005;6:118.
58. Arribere JA, Bell RT, Fu BX, Artiles KL, Hartman PS, Fire AZ. Efficient marker-free recovery of custom genetic modifications with CRISPR/Cas9 in Caenorhabditis elegans. Genetics. 2014;198(3):837-46.
59. Andrusiak MG, Sharifnia P, Lyu X, Wang Z, Dickey AM, Wu Z, et al. Inhibition of Axon Regeneration by Liquid-like TIAR-2 Granules. Neuron. 2019;104(2):290-304 e8.
60. McReynolds MR, Wang W, Holleran LM, Hanna-Rose W. Uridine monophosphate synthetase enables eukaryotic de novo NAD(+) biosynthesis from quinolinic acid. J Biol Chem. 2017;292(27):11147-53.

61. Djonović S, Urbach JM, Drenkard E, Bush J, Feinbaum R, Ausubel JL, et al. Trehalose biosynthesis promotes Pseudomonas aeruginosa pathogenicity in plants. PLoS Pathog. 2013;9(3):e1003217.
62. Afgan E, Baker D, Batut B, van den Beek M, Bouvier D, Cech M, et al. The Galaxy platform for accessible, reproducible and collaborative biomedical analyses: 2018 update. Nucleic Acids Res. 2018;46(W1):W537-w44.

Figure Legends

Fig 1. *pnp-1* mutants have increased expression of IPR genes

A) Gene structure of the two isoforms of *pnp-1* with exons indicated as black boxes. 5' and 3' untranslated regions are not shown. B-D) *pals-5p::GFP* IPR reporter expression in wild-type animals, *pnp-1(jy90)* and *pnp-1(jy121)* mutants. *myo-2p*::*mCherry* is a pharyngeal marker for the presence of the IPR reporter transgene. Scale bar is 100 μm. E) qRT-PCR of a subset of IPR genes in *pnp-1(jy90)* and *pnp-1(jy121)* mutants. Fold change in gene expression is shown relative to wild-type animals. Graph shows the mean fold change of three independent experiments. Error bars are standard deviation (SD). Mixed stage populations of animals were used. **** indicates $p < 0.0001$ by one-tailed t-test. F) Quantification of inosine and hypoxanthine levels in *pnp-1* and *pals-22* mutants from metabolomics analysis. Graph shows the mean levels of metabolites from six independent experiments for *pnp-1(jy121)*, *pnp-1(jy90)* and *pals-22(jy1)* mutants, and five independent experiments for wild-type animals. Error bars are standard error of the mean (SEM). **** indicates $p < 0.0001$ by one-way ANOVA. E,F) Red dots indicate values from individual experiments. See materials and methods for more information.

Fig 2. *pnp-1* regulates intracellular pathogen resistance

A) qRT-PCR for Orsay viral load in wild-type animals, *pnp-1(jy90)*, *pnp-1(jy121)* and *pals-22(jy1)* mutants. Fold change in gene expression is shown relative to wild-type animals. Graph shows results of four independent experiments. Mean is shown with error bars as SD. Synchronized fourth larval stage (L4) animals were used. **** indicates $p < 0.0001$ by one-tailed t-test. B) Quantification of *N. parisii* sporoplasm number in wild-type animals, *pnp-1(jy90)*, *pnp-1(jy121)* and *pals-22(jy1)* first larval stage

(L1) mutants at 3 hpi. n=225 animals per genotype. Box represents 50% of the data closest to the median while whiskers span the values outside the box. C) Quantification of *N. parisii* pathogen load in wild-type animals, *pnp-1(jy90)*, *pnp-1(jy121)* and *pals-22(jy1)* L1 mutants at 30 hpi. n=300 animals per genotype. *N. parisii* load per animal was quantified with the COPAS Biosort machine and normalized to time-of-flight as proxy for the length of the animal. Graph shows combined results of three independent experiments. Mean is shown with error bars as SD. B, C) *N. parisii* was visualized using an *N. parisii* rRNA specific probe. Each graph shows the combined results of three independent experiments. D) Survival of wild-type, *pnp-1(jy90)* and *pnp-1(jy121)* mutants after infection with *N. parisii*. n=120 per genotype. One experiment of four independent experiments is shown (see Supplemental Figure 3 for additional three experiments). E) Quantification of fluorescent bead accumulation in wild-type animals, *pnp-1(jy90)*, *pnp-1(jy121)* and *eat-2(ad465)* mutants. n=150 animals per genotype. The corrected total fluorescence (CTF) per worm was calculated and normalized to worm area. Graph shows combined results of three independent experiments. Mean is shown with error bars as standard error of the mean. B-E) **** indicates $p < 0.0001$ by one-way ANOVA.

Fig 3. *pnp-1* functions in the intestine to regulate the IPR

A) Expression of *PNP-1*::*EGFP::3XFLAG* under control of the wild-type *pnp-1* genomic locus. Asterisks indicate intestines, arrows indicate neurons. Scale bar is 100 μm. B) Quantification of *N. parisii* sporoplasm number at 3 hpi in *pnp-1* mutants containing the rescuing *pnp-1*::*EGFP::3XFLAG* genomic locus in L1 animals (indicated as "+WT *pnp-1*"), as well as their non-transgenic siblings (indicated as "-WT *pnp-1*"). n=255 animals per genotype. C) Quantification of *N. parisii* sporoplasm number at 3 hpi in *pnp-1* mutants containing wild-type *pnp-1* cDNA under the control the *vha-6* (intestinal) or *unc-119* (neuronal) promoters in L1 animals). n=150 per genotype. B, C) *N. parisii* was visualized using an *N. parisii* rRNA specific probe. Box represents 50% of the data closest to the median while whiskers span the values outside the box. Each graph shows the combined results of three independent experiments. In the graphs, the box represents the 50% of the data closest to the median while the whiskers span the

values outside the box. **** indicates p < 0.0001 by one-way ANOVA. D) qRT-PCR of a subset of IPR genes in adult *pnp-1* mutants containing wild-type *pnp-1* cDNA under the control the *vha-6* or *unc-119* promoter. Fold change in gene expression is shown relative to control. Graphs show the combined results of three independent experiments. **** indicates p < 0.0001 by one-tailed t-test.

Fig 4. Lifespan, thermotolerance and *P. aeruginosa* resistance phenotypes of *pnp-1* mutants

A) Lifespan of wild-type animals, *pnp-1(jy90)* and *pnp-1(jy121)* mutants. n=90 animals per genotype. Results from one representative experiment of four independent experiments is shown (see S5 Fig for additional three experiments). Survival of each mutant population was compared to that of the wild-type population with the Log-rank (Mantel-Cox) test. B) Survival of wild-type animals, *pnp-1(jy90)* and *pnp-1(jy121)* mutants 24 hours after 2 hour 37^{o}C heat shock. C) Survival of wild-type animals, *pnp-1(jy90), pals-22(jy1)* and *pals-22(jy1); pnp-1(jy90)* mutants 24 hours after 2 hour 37^{o}C heat shock. B,C) For one experiment, three plates per genotype with 30 worms per plate were tested. One dot represents the survival from one plate. The graphs show the mean survival of three independent experiments. Error bars are SD. D) Quantification of PA14-dsRED pathogen load in L4 stage wild-type animals, *pnp-1(jy90)* and *pnp-1(jy121)* mutants at 16 hpi. E) Quantification of PA14-dsRED pathogen load in L4 stage wild-type animals, *pnp-1(jy90)*, *pals-22(jy1), pmk-1(km25), pnp-1(jy90) pmk-1(km25)* and *pals-22(jy1); pmk-1(km25)* mutants at 16 hpi. D, E) PA14-dsRED red fluorescence per animal was quantified with the COPAS Biosort machine and normalized to time-of-flight as proxy for the length of the animal. Graph shows the combined results of three independent experiments. Each dot represents an individual animal. Mean is shown with error bars as SD. F) Quantification of *N. parisii* sporoplasm number in wild-type animals, *pnp-1(jy90)*, *pals-22(jy1), pmk-1(km25), pnp-1(jy90) pmk-1(km25)* and *pals-22(jy1); pmk-1(km25)* mutants at 3 hpi. n=400 animals per genotype. *N. parisii* was visualized using an *N. parisii* rRNA specific probe. Each dot represents an individual animal, and the graph shows the combined results of four independent experiments.

The box represents the 50% of the data closest to the median while the whiskers span the values outside the box. B-E) **** indicates $p < 0.0001$ by one-way ANOVA.

Fig 5. RNA-seq analysis demonstrates that *pnp-1* represses expression of many IPR genes

A) Venn diagram of differentially expressed genes in *pnp-1(jy90)* and *pnp-1(jy121)* mutants as compared to wild-type animals. Both up (rf = 31.5; $p < 0.000e+00$) and down (rf = 239.6; $p < 3.489e-58$) regulated genes have significant overlap between the two mutant alleles (S6 Table). B) Venn diagram of upregulated genes in *pnp-1(jy90)*, *pnp-1(jy121)* and *pals-22(jy3)* mutants as compared to wild-type animals. Upregulated genes in both *pnp-1(jy90)* (rf = 2.9; $p < 4.566e-62$) and *pnp-1(jy121)* (rf = 2.8 ; $p < 1.591e-52$) mutants have significant overlap with those upregulated in *pals-22(jy3)* mutants from a previous study (S6 Table) [17]. A, B) rf is the ratio of actual overlap to expected overlap where rf > 1 indicates overrepresentation and rf < 1 indicates underrepresentation. C) Log2 fold-change of *pals* genes in *pnp-1(jy90)* and *pnp-1(jy121)* mutants normalized to wild-type. D) Log2 fold change of a subset of non-*pals* genes in *pnp-1(jy90)* and *pnp-1(jy121)* mutants normalized to wild-type. E) Correlation between genes differentially expressed by various known IPR activators and those differentially expressed in *pnp-1(jy90)* or *pnp-1(jy121)* mutants. F) Wormcat analysis for significantly enriched categories in differentially expressed gene sets of *pnp-1(jy90)* and *pnp-1(jy121)* mutants. Size of the circles indicates the number of the genes and color indicates value of significant over representation in each Wormcat category. G) Correlation of genes differentially expressed by bacterial pathogens, immune regulators, and various stressors to those differentially expressed in *pnp-1(jy90)* or *pnp-1(jy121)* mutants. E, G) Analysis was performed using GSEA 3.0 software, and correlations of genes sets (S4 Table) were quantified as a Normalized Enrichment Score (NES) (S5 Table). NES's presented in a heat map. Blue indicates significant correlation of downregulated genes in a *pnp-1* mutant with the tested gene set, yellow indicates significant correlation of upregulated genes in a *pnp-1* mutant with the tested gene set, while black indicates no significant correlation ($p > 0.05$ or False Discovery Rate < 0.25).

Fig 6. Model for *pnp-1* regulation of immune responses

A) *pnp-1* negatively regulates mRNA expression of IPR genes induced by infection with the intracellular pathogens the Orsay virus and *N. parisii* (microsporidia). Loss of *pnp-1* or *pals-22* results in constitutive expression of IPR genes and resistance to the Orsay virus and *N. parisii*. *pmk-1 (*p38 MAPK) mutants display increased susceptibility to *N. parisii* as compared to wild-type animals. Because IPR genes are distinct from *pmk-1*-regulated genes, and *pnp-1* mutant resistance does not require *pmk-1*, we favor a model where *pmk-1* acts in parallel to the IPR. B) *pnp-1* negatively regulates genes that are induced by various extracellular pathogens and *pnp-1* mutants are resistant to infection by the extracellular Gram-negative pathogen *P. aeruginosa*. Resistance to *P. aeruginosa* in *pnp-1* mutants requires *pmk-1*, and *pnp-1* mutants have upregulation of genes induced by wild-type *pmk-1*, suggesting that here, *pnp-1* functions upstream of *pmk-1*.

Supplemental Figure Legends

S1 Fig. Alignment of PNP proteins across species

Alignment of PNP protein sequences from *C. elegans* (two isoforms, PNP-1a and PNP-1b), *Drosophila melanogaster* (DmPNP), *Mus musculus* (MsPNP) and *Homo sapiens* (HsPNP). Similar amino acids shaded gray, identical amino acids shaded black. Red indicates the serine converted to leucine in *pnp-1* mutants. Clustal Omega was used to perform the alignment (https://www.ebi.ac.uk/Tools/msa/clustalo/). BoxShade (https://embnet.vital-it.ch/software/BOX_form.html) was used to annotate sequence homology.

S2 Fig. Quantification by LC-MS of purine metabolites in *pnp-1* and *pals-22* mutants

A) Schematic of purine synthesis pathways with select metabolites included. The degradation pathway is highlighted in red. The de novo pathway and metabolites is highlighted in blue. Metabolites that are not highlighted are common to both pathways.

B-D) Quantification of adenosine, de novo specific metabolites and purine nucleotides, respectively (inosine and hypoxanthine are shown in Fig 1F). Graphs show the mean amount (in log10 scale) of the metabolites of six independent experiments for *pnp-1(jy121)*, *pnp-1(jy90)* and *pals-22(jy1)* mutants and five independent experiments wild-type animals. Red dots show individual values for each experiment. Error bars are SEM. Unless otherwise indicated, there is no significant difference in metabolite amounts in *pnp-1* mutants or *pals-22* mutants compared to control as determined by one-way ANOVA. * indicates $p < 0.05$. Abbreviations used: R5P is ribose-5-phospate; GAR is glycineamide ribonucleotide; CAIR is 5'-phosphoribosyl-4-carboxy-5-aminoimidazole; SAICAR is succinylaminoimidazole carboxamide ribotide; AICAR is 5-Aminoimidazole-4-carboxamide ribonucleotide; IMP is inosine monophosphate; XMP is xanthine monophosphate; GMP is guanosine monophosphate; S-AMP is adenylosuccinate; AMP is adenosine monophosphate.

S3 Fig. Individual experiments for survival of wild-type, *pnp-1(jy90)* and *pnp-1(jy121)* after *N. parisii* infection

S4 Fig. DiI filling of animals expressing *pnp-1::EGFP::3XFLAG*

Transgenic *pnp-1*::*EGFP::3XFLAG* TransgeneOme animals, stained with the lipophilic fluorescent dye DiI, which labels amphid neurons in red. GFP-expressing cells (indicated by green arrows) are distinct from DiI-labled cells (indicated by red arrows), suggesting that *pnp-1* is not expressed in amphid neurons. Each row is an individual animal and scale bar is 20 μm. The head of the animal is shown with anterior to the left. Worm bodies are outlined in white. Asterisks indicate GFP-expressing intestines. The exposure time for GFP in the bottom row is higher than that of the above two panels to better visualize the GFP-expressing processes extending anteriorly.

S5 Fig. Individual experiments for lifespan of wild-type animals, *pnp-1(jy90)* and *pnp-1(jy121)* mutants

Supplementary Tables

S1 Table. Lists of strains, plasmids and primers

S2 Table. RNA-seq statistics

S3 Table. Differentially expressed genes lists

S4 Table. Gene sets used for GSEA

S5 Table. Detailed GSEA results

S6 Table. Detailed results of hypergeometric testing

S7 Table. Detailed GO Term results

S8 Table. Detailed Wormcat results

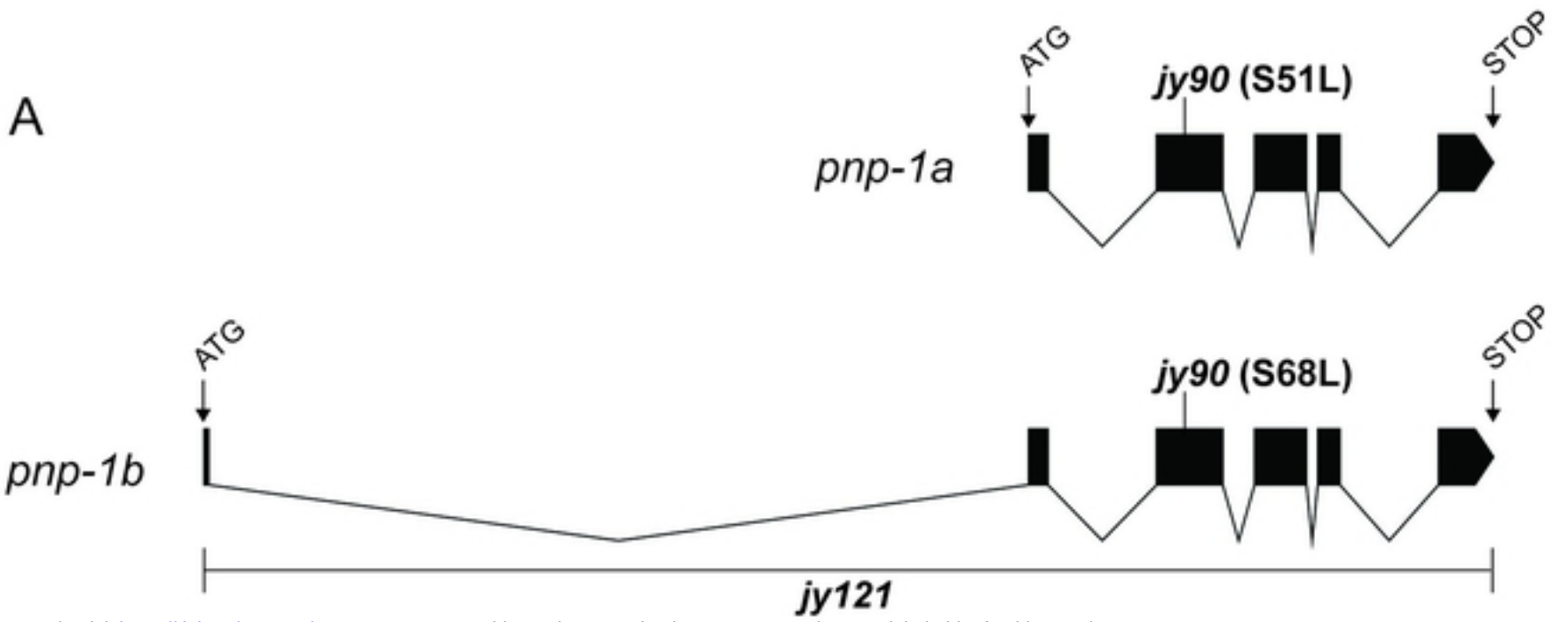

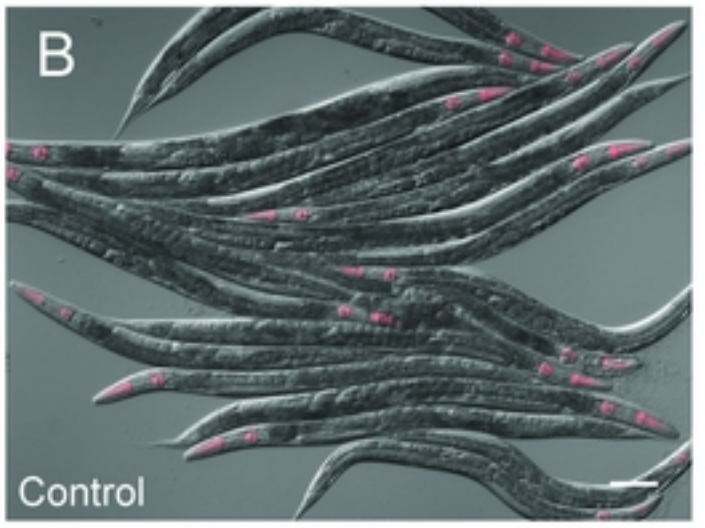

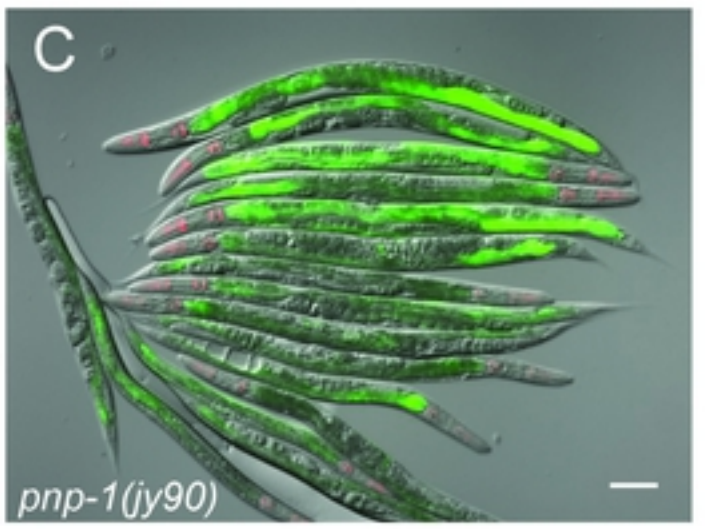

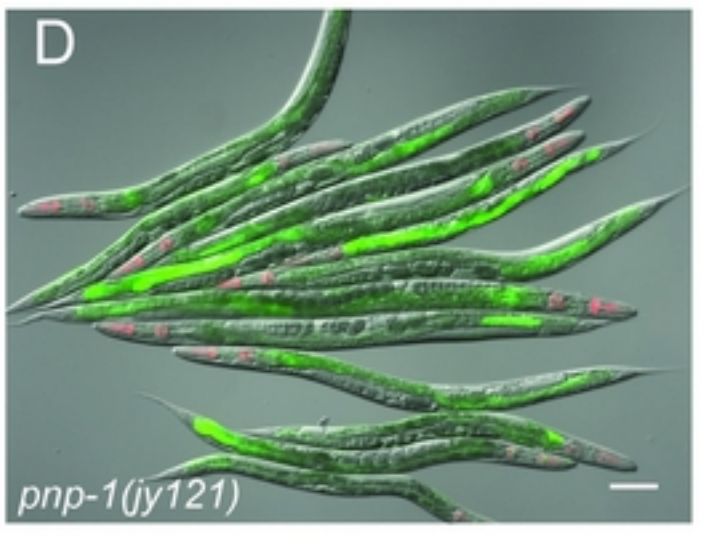

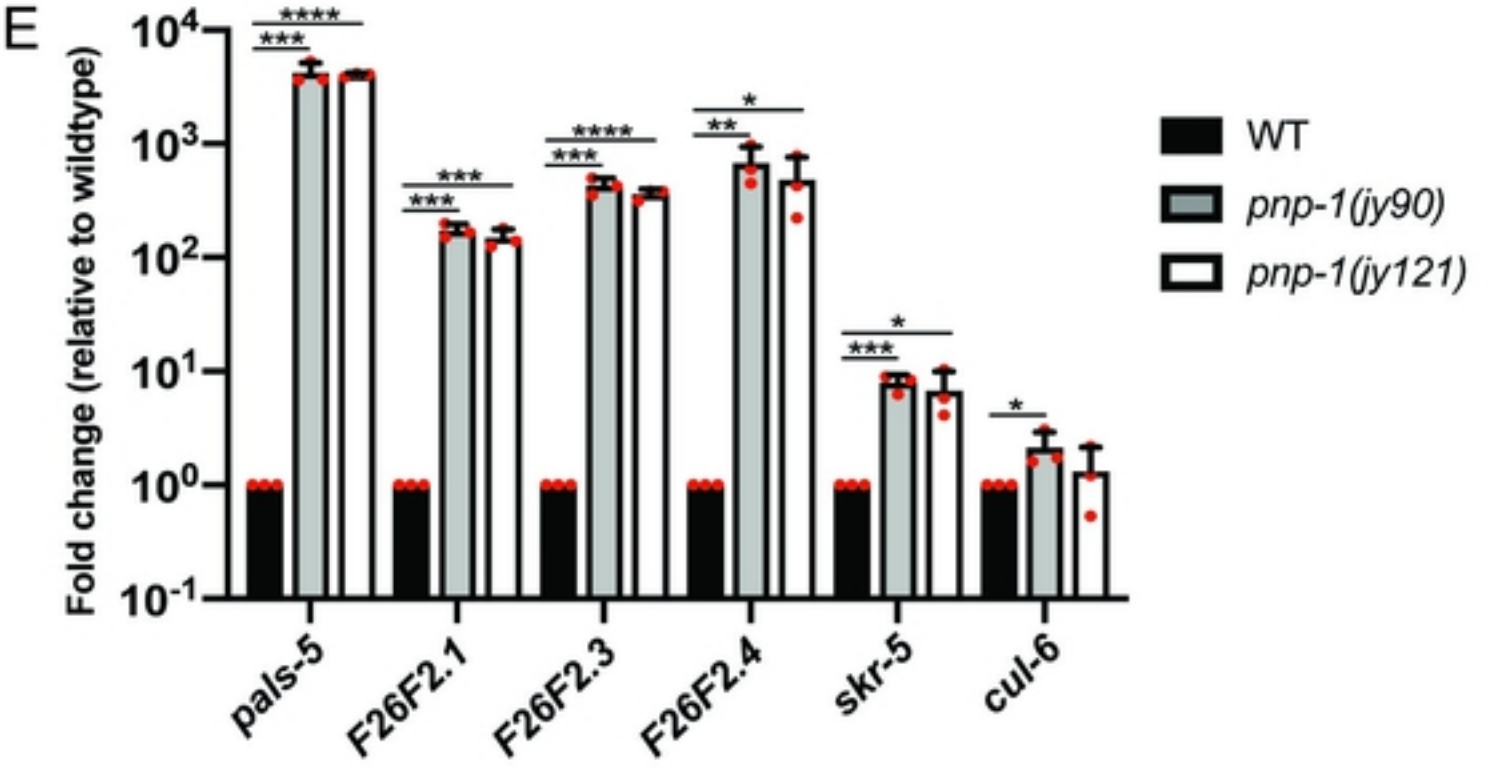

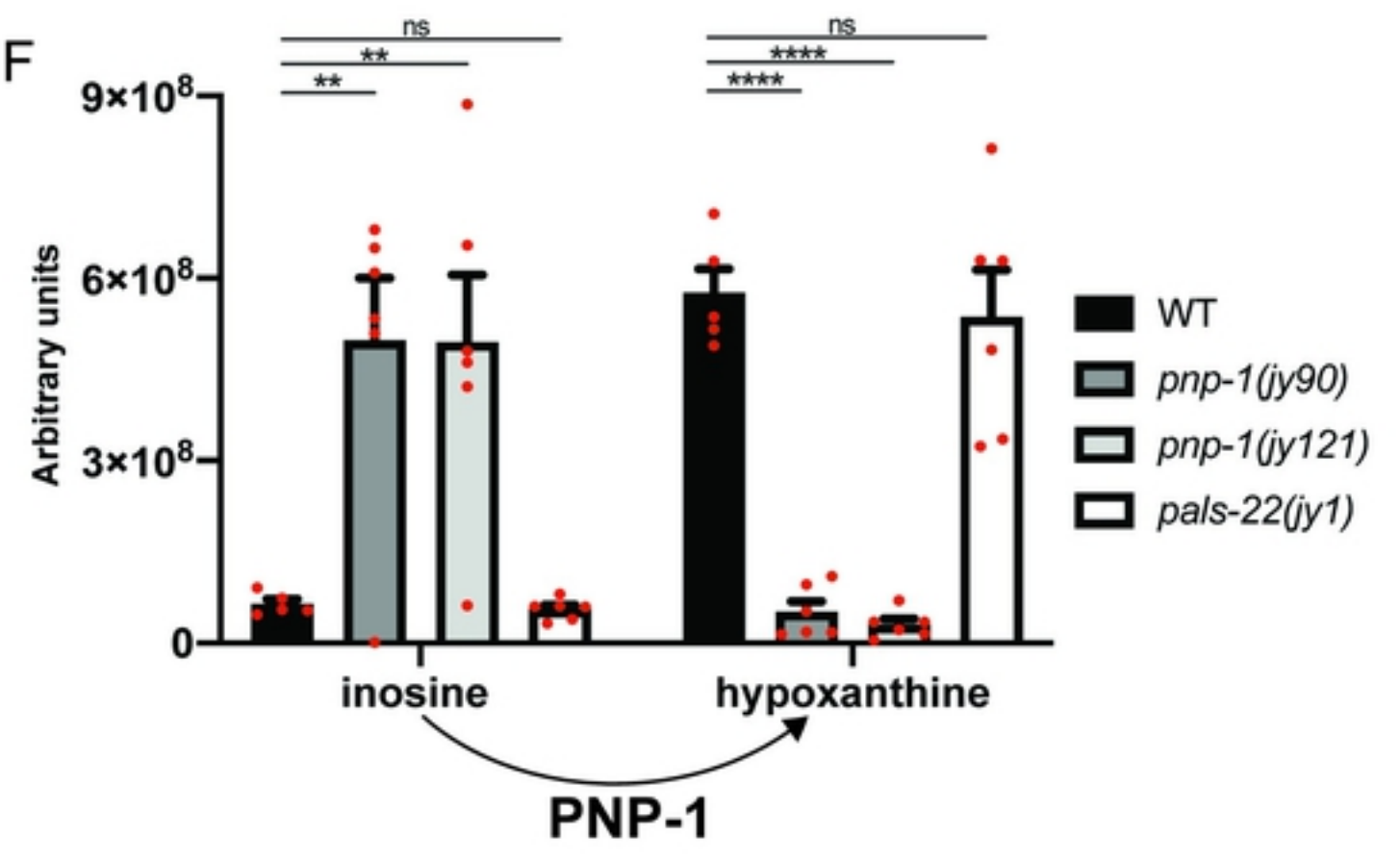

Fig 1

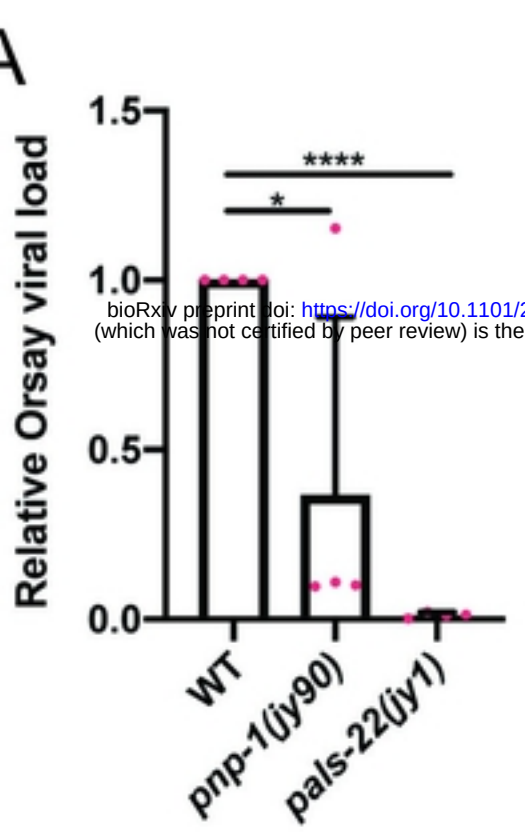

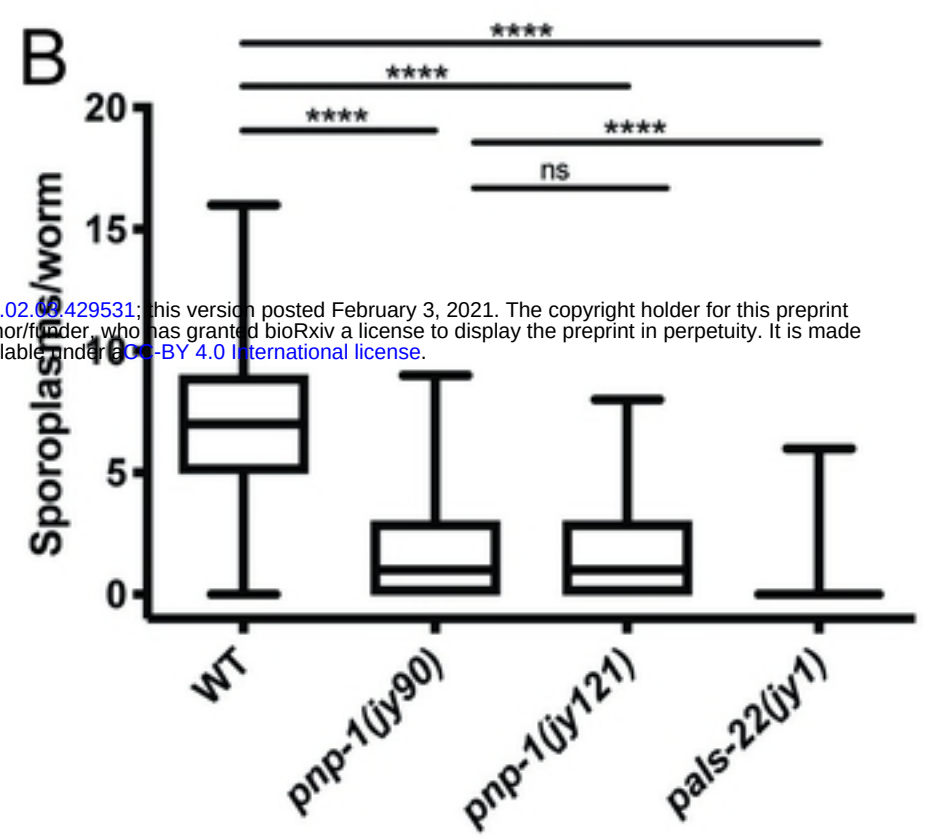

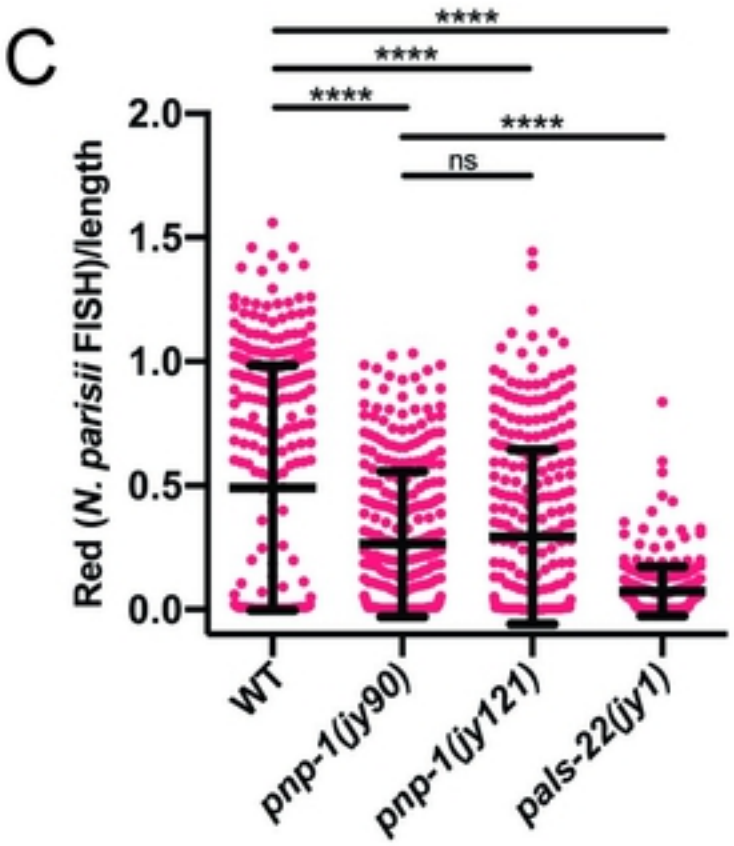

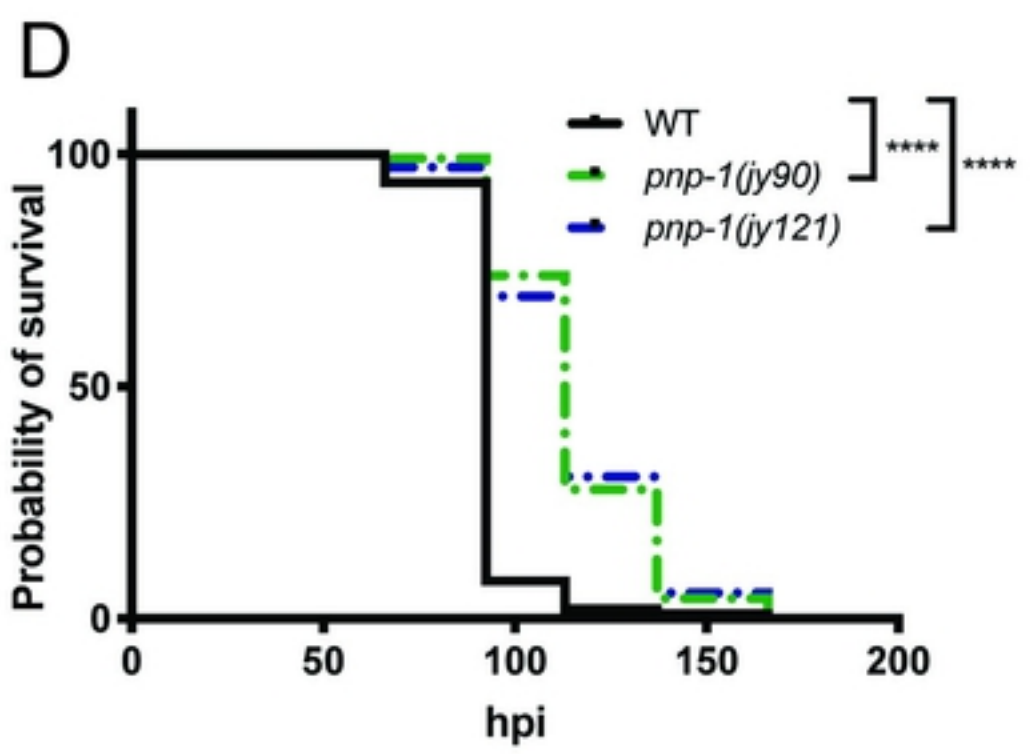

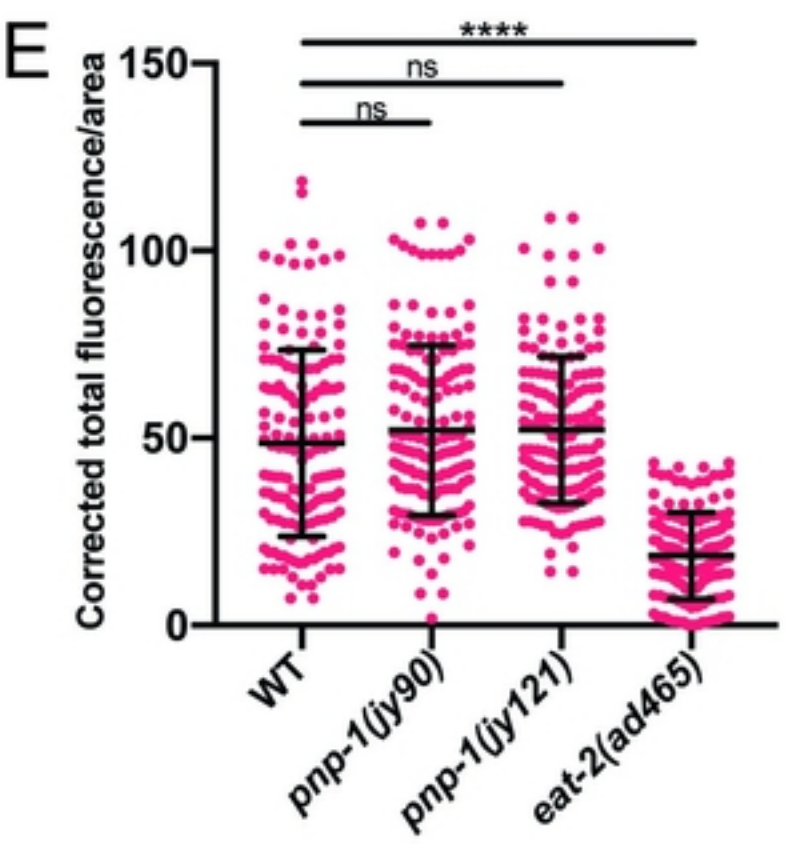

Fig 2

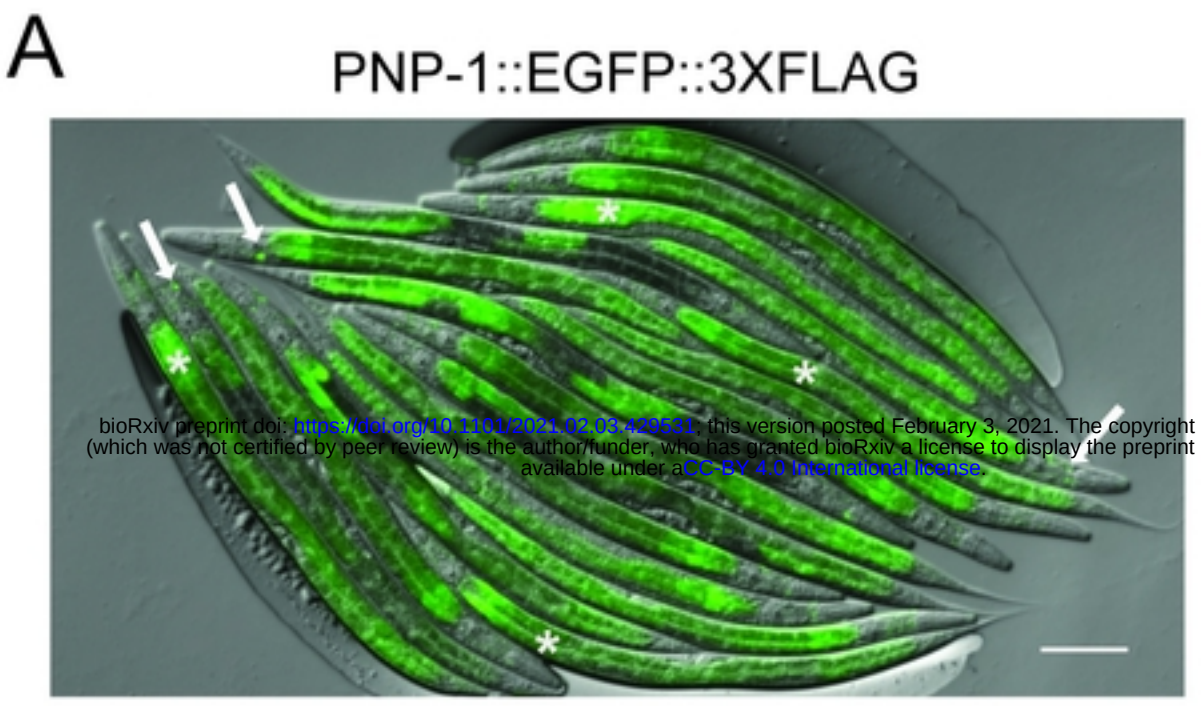

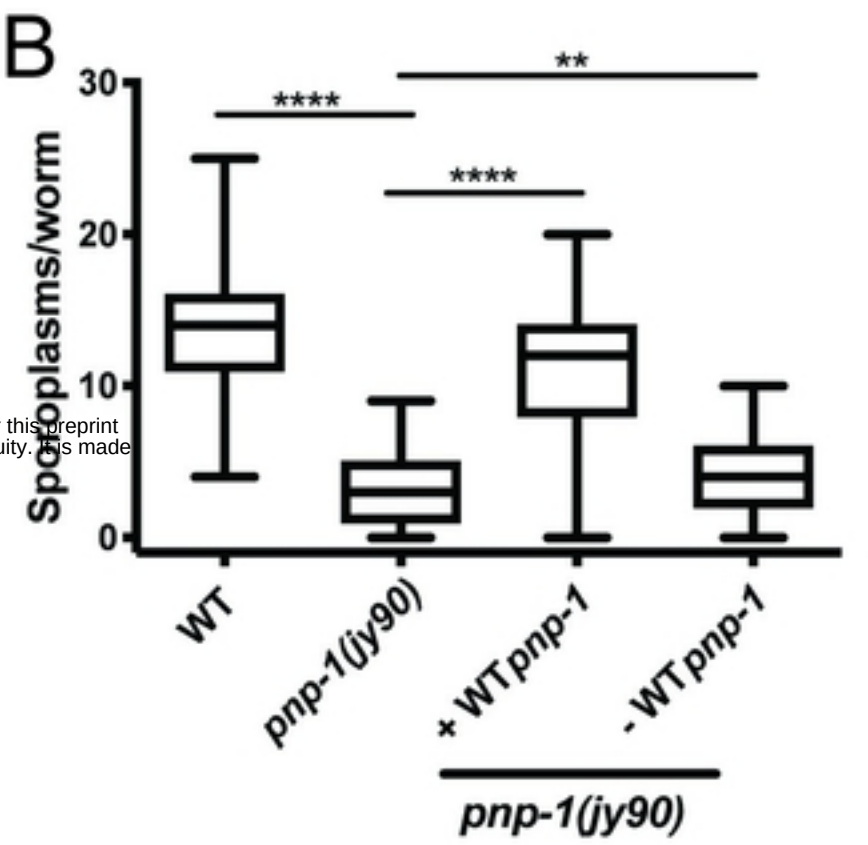

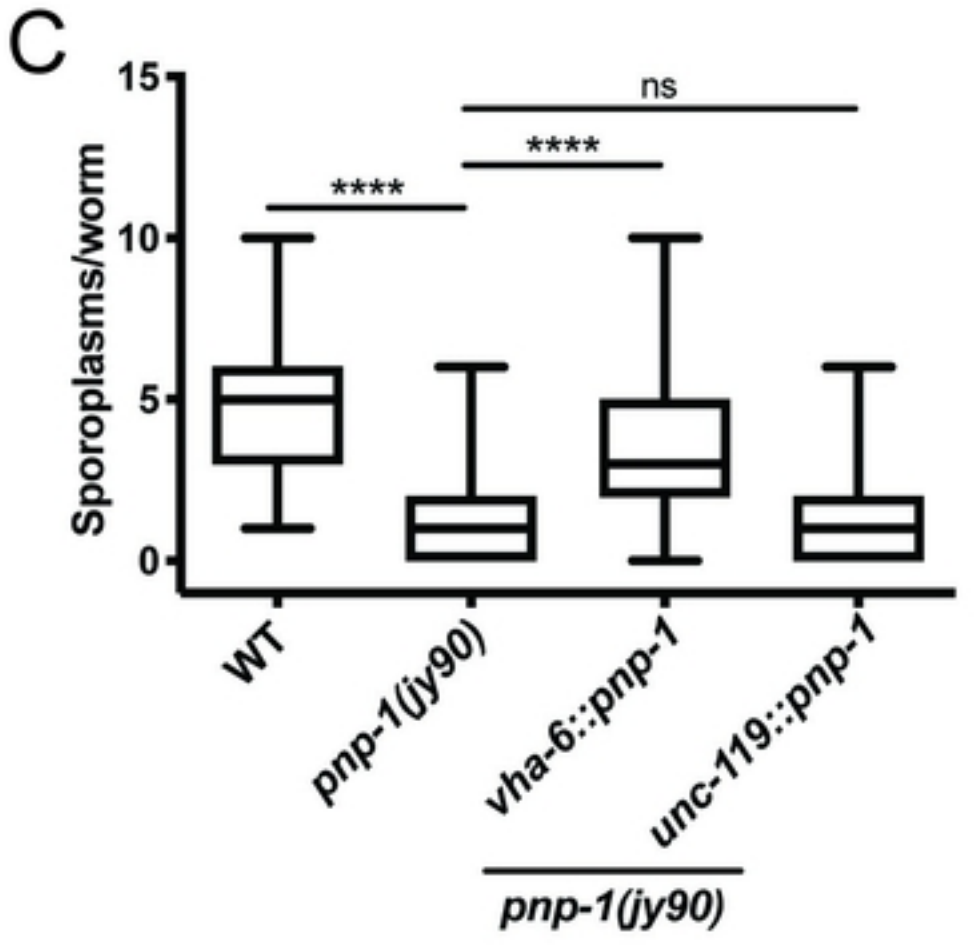

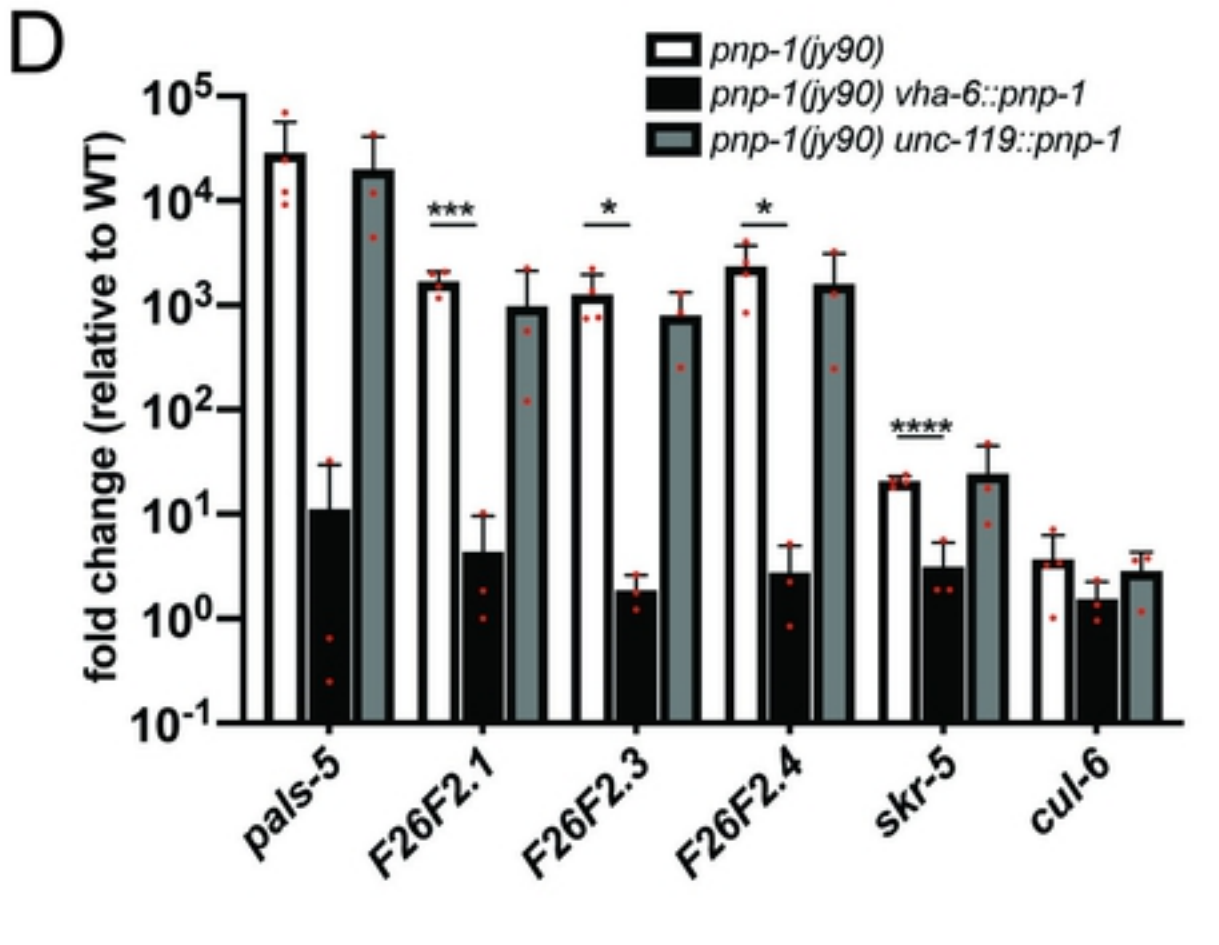

Fig 3

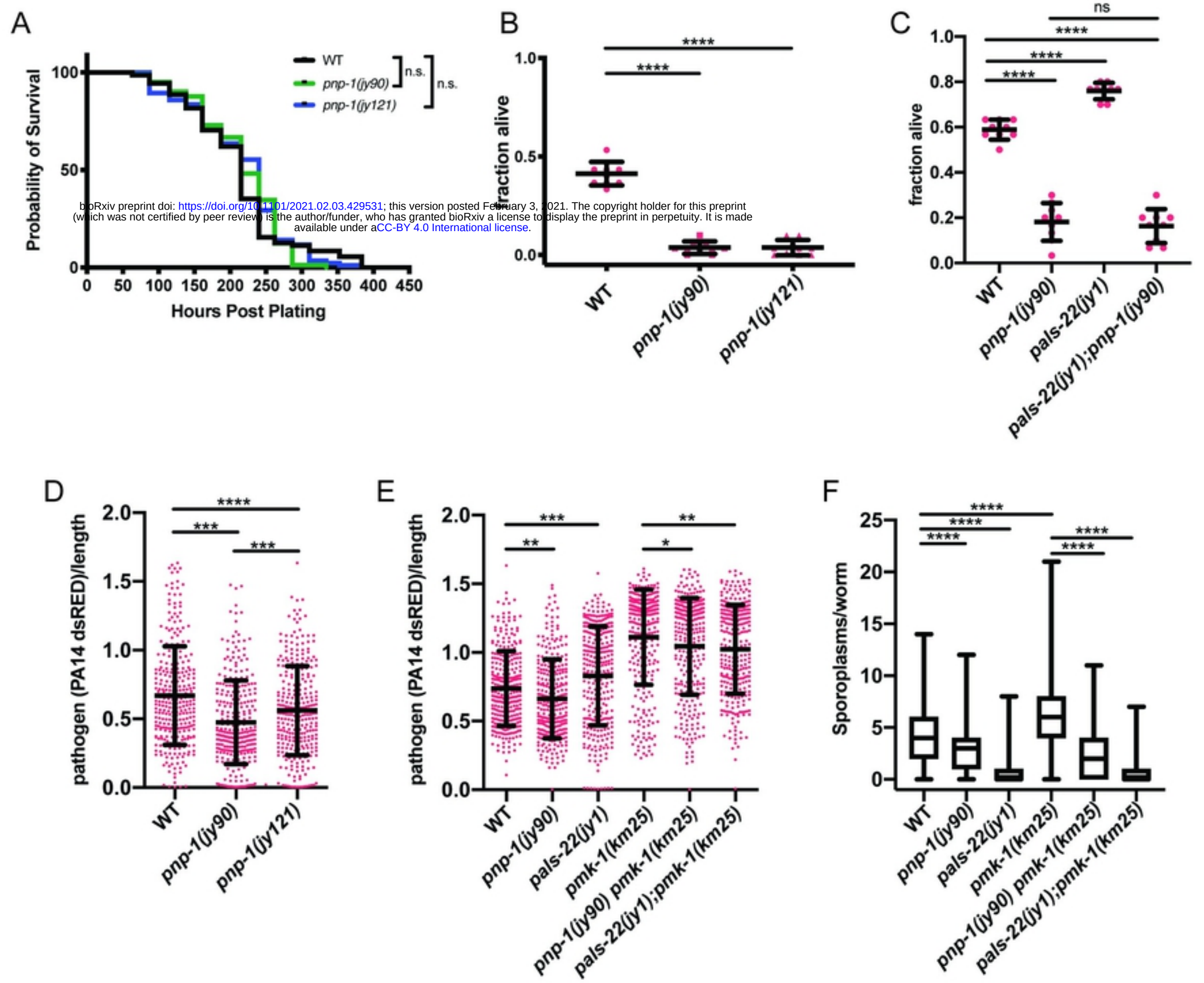

Fig 4

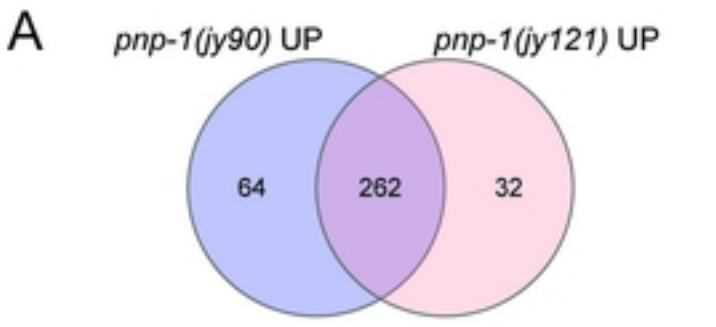

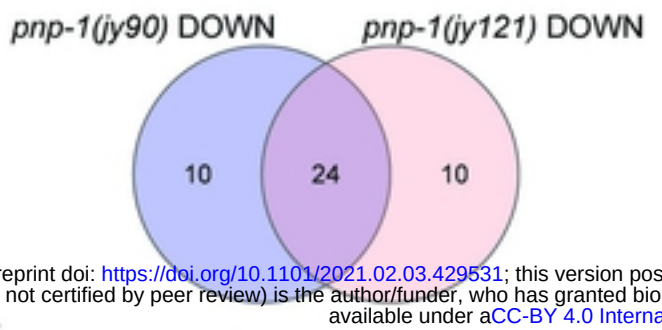

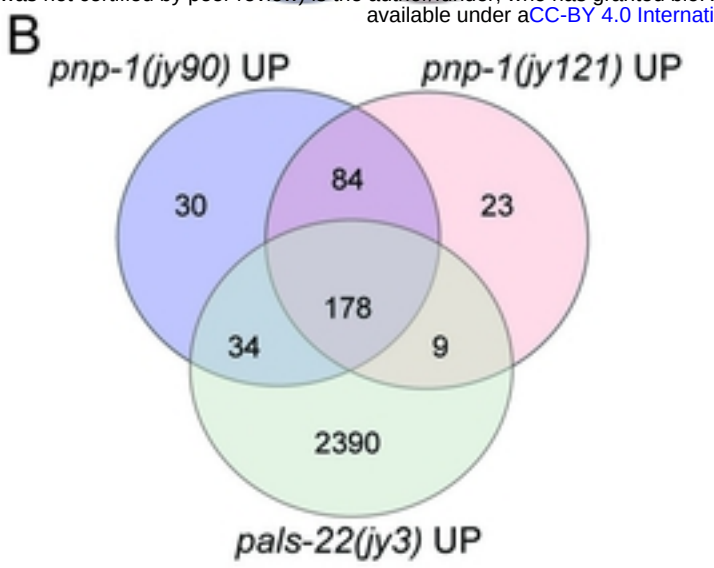

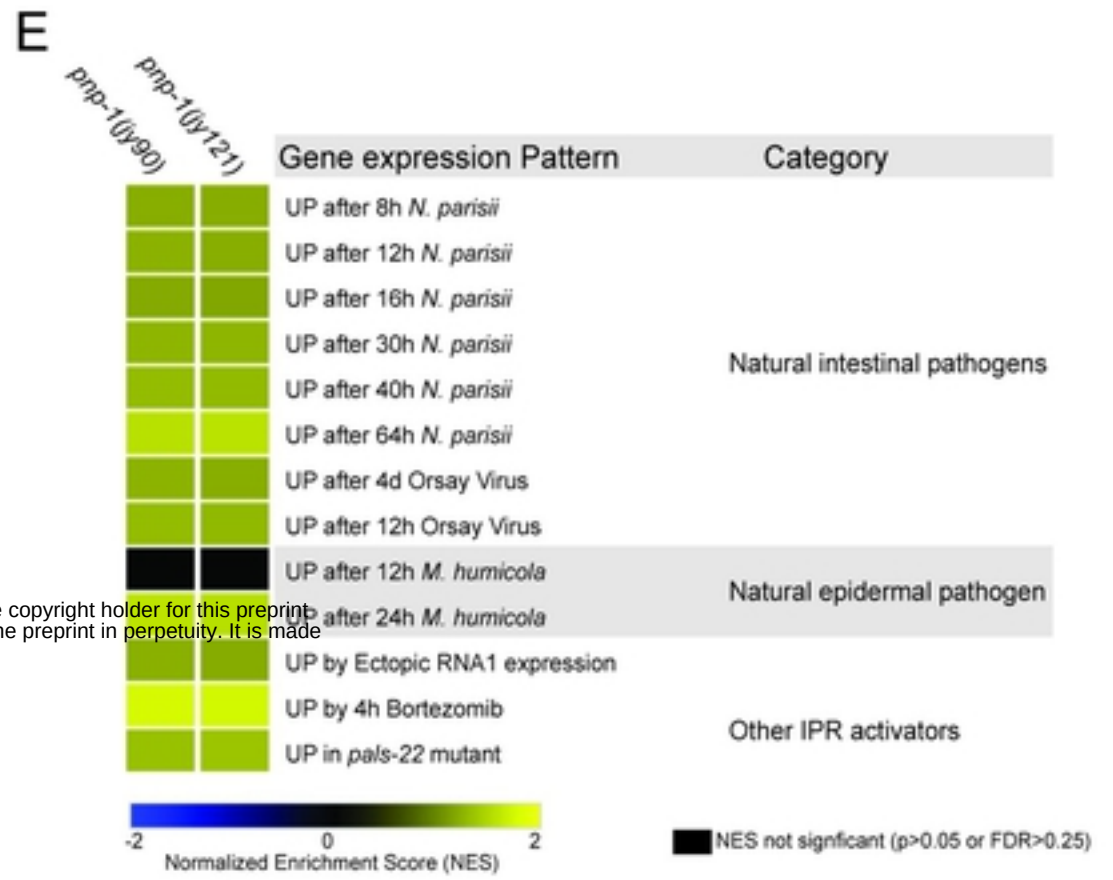

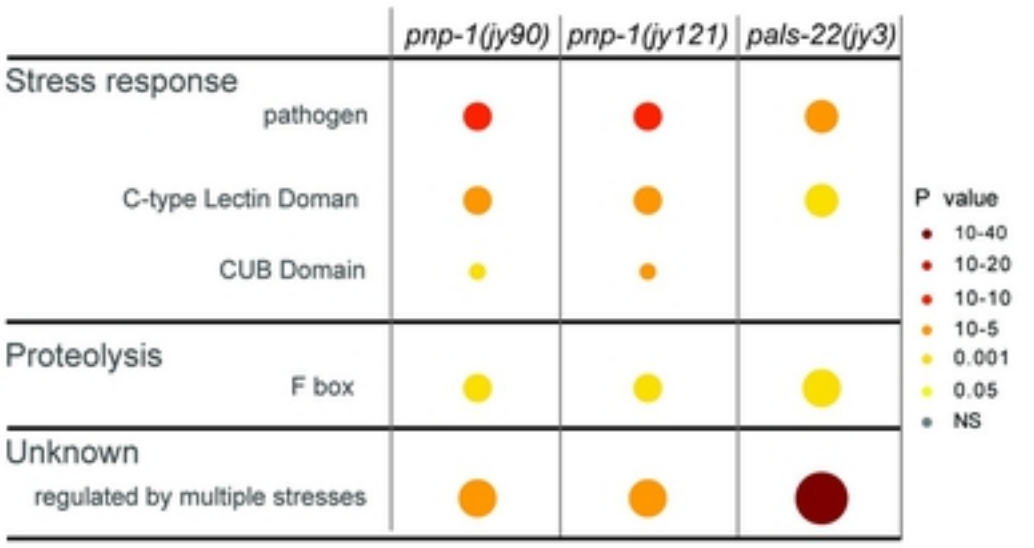

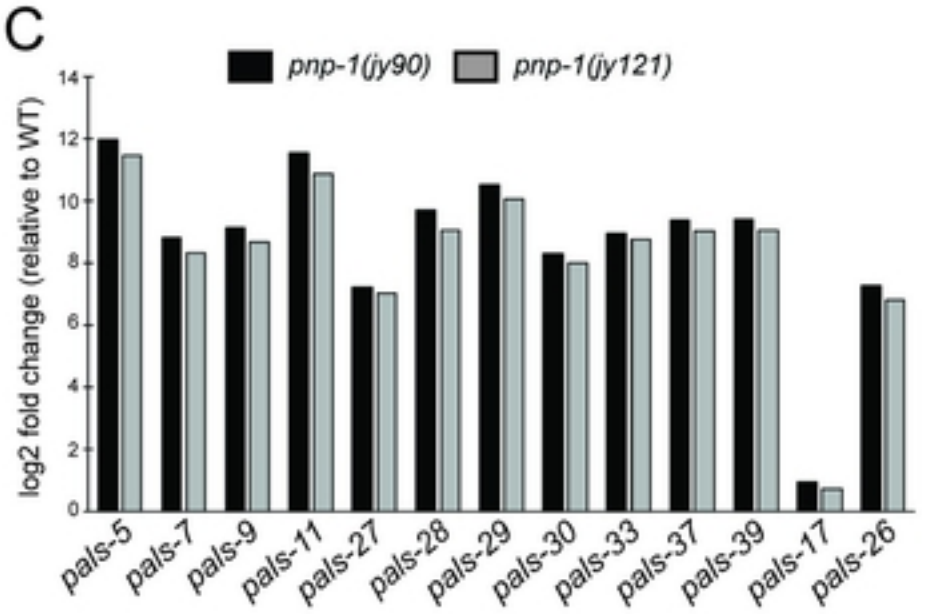

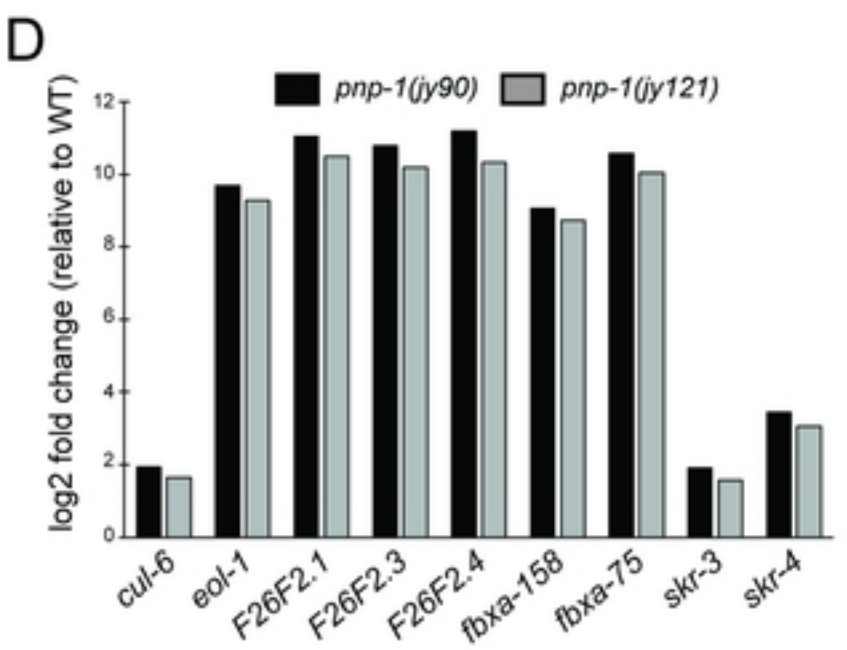

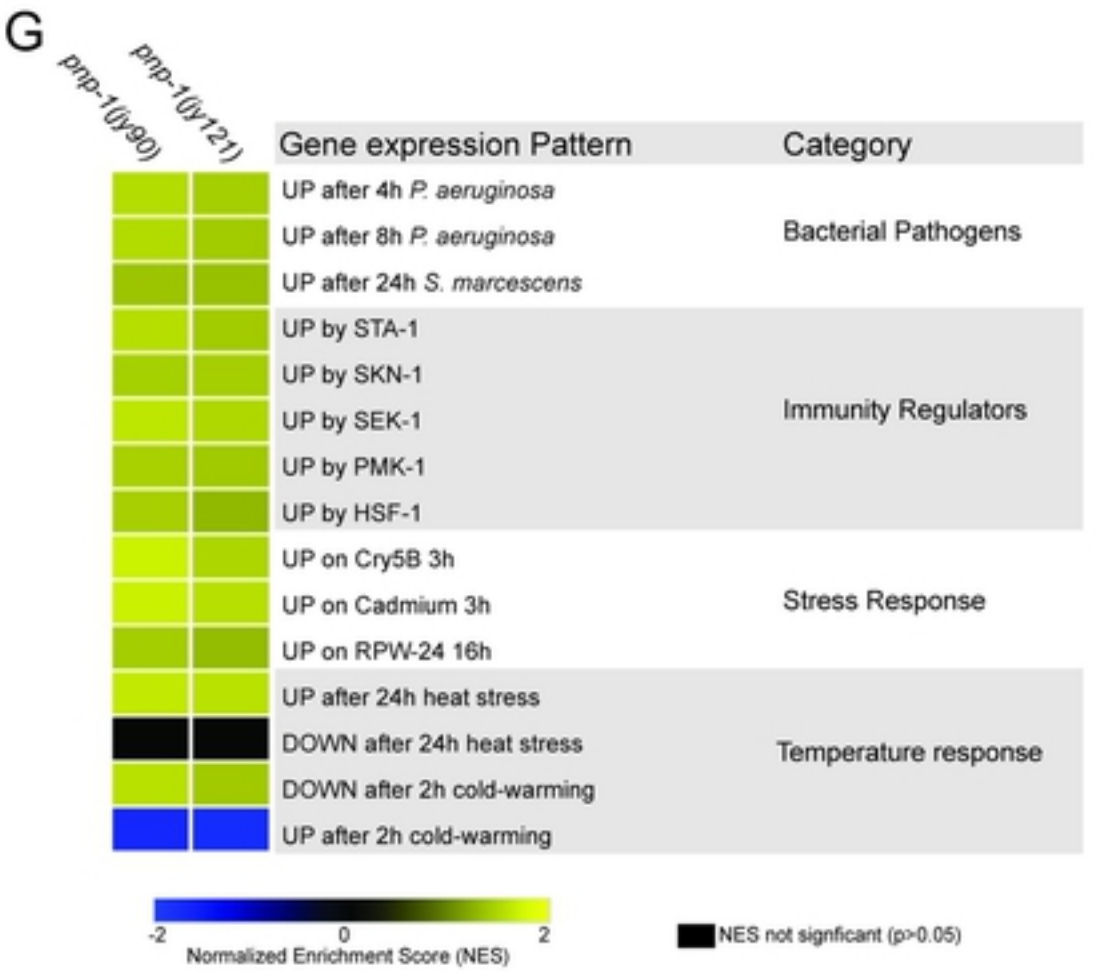

Fig 5

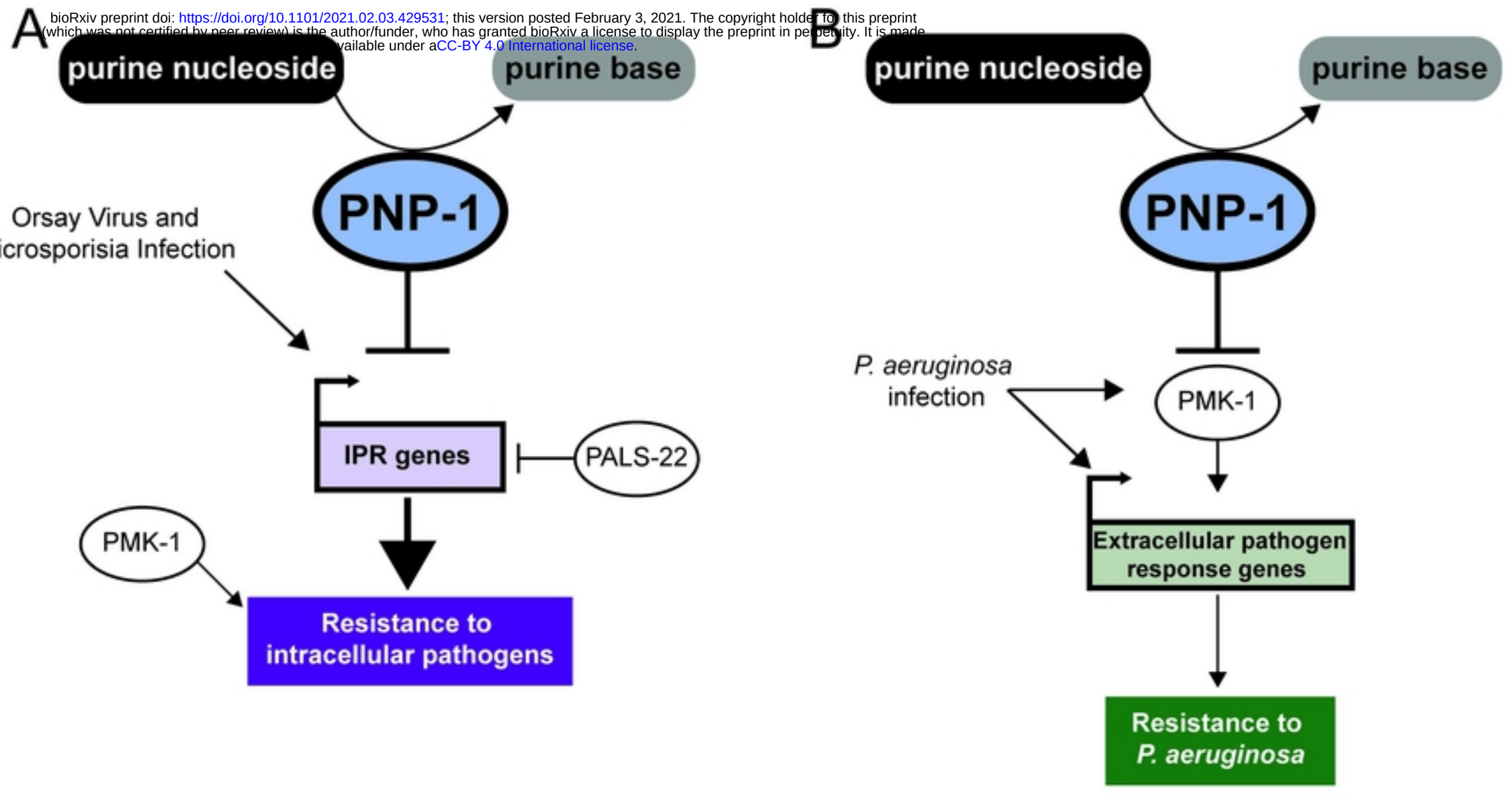

Fig 6

```
PNP-1a      1 ------------------------------------------------------------
PNP-1b      1 ------------------------------------------------------------M
DmPNP       1 MTGYKVANGNGHSNGNGNTKGTNGTNGHSNGHKSADYTAQENPTMCSRDCCSGPGGSNRG
MsPNP       1 ------------------------------------------------------------
HsPNP       1 ------------------------------------------------------------

PNP-1a      1 -------------------------M---ENNNSPTNAAEH--------NQKIDPRNYDDVLSV
PNP-1b      2 GNCTQKLTTS------TSLSPAM---ENNNSPTNAAEH--------NQKIDPRNYDDVLSV
DmPNP      61 NTCSDKKGAKAGSLTGEKIIPTPQSLLGNGKIQCELTHEELRALRVLNEDTYPYEVIEEI
MsPNP       1 ------------------------------------------------MENEFTYEDYETT
HsPNP       1 ------------------------------------------------MENGYTYEDYKNT

PNP-1a     29 AASIREQVGEDVARADLGIICGSGLGPIGDTVQDATILPYSKIPGFPTTHVVGHKGNMIF
PNP-1b     46 AASIREQVGEDVARADLGIICGSGLGPIGDTVQDATILPYSKIPGFPTTHVVGHKGNMIF
DmPNP     121 ADFI---TKGSGMRPKIGIICGSGLGSLADMIQDPKIFEYEKIPNFPVSTVEGHAGRLVV
MsPNP      14 AKWL---LQHTEYRPQVAVICGSGLGGLTAHLKEAQIFDYNEIPNFPQSTVQGHAGRLVF
HsPNP      14 AEWL---LSHTKHRPQVAIICGSGLGGLTDKLTQAQIFDYGEIPNFPRSTVPGHAGRLVF

PNP-1a     89 GKLGGKKVVCLQGRFHPYEHNMDLALCTLPVRVMHQLGIKIMIVSNAAGGINAVLRHGDL
PNP-1b    106 GKLGGKKVVCLQGRFHPYEHNMDLALCTLPVRVMHQLGIKIMIVSNAAGGINAVLRHGDL
DmPNP     178 GTLEGATVMAMQGRFHFYEG-YPLAKCSMPVRVMKLCGVEYLFATNAAGGINPRFAVGDI
MsPNP      71 GLLNGRCCVMMQGRFHMYEG-YSLSKVTFPVRVFHLLGVETLVVTNAAGGLNPNFEVGDI
HsPNP      71 GFLNGRACVMMQGRFHMYEG-YPLWKVTFPVRVFHLLGVDTLVVTNAAGGLNPKFEVGDI

PNP-1a    149 MLIKDHIFLPALAGFSPLVGCNDPRFGARFVSVHDAYDKQLRQLAIDVGRR--SDMTLYE
PNP-1b    166 MLIKDHIFLPALAGFSPLVGCNDPRFGARFVSVHDAYDKQLRQLAIDVGRR--SDMTLYE
DmPNP     237 MLMHDHVNMLGFAGNSPLQGPNDPRFGPRFPALVNSYNKDLINKAIEIAKAMGIESNIHV
MsPNP     130 MLIRDHINLPGFCGQNPLRGPNDERFGVRFPAMSDAYDRDMRQKAFTAWKQMGEQRKLQE
HsPNP     130 MLIRDHINLPGFSGQNPLRGPNDERFGDRFPAMSDAYDRTMRQRALSTWKQMGEQRELQE

PNP-1a    207 GVYVMSGGPQYESPAEVSLFKTVGADALGMSTCHEVTVARQCGIKVLGFSLITNIANLDA
PNP-1b    224 GVYVMSGGPQYESPAEVSLFKTVGADALGMSTCHEVTVARQCGIKVLGFSLITNIANLDA
DmPNP     297 GVYSCLGGPNYETIAELKALRMMGVDAVGMSTVHEVITARHCDMKVFAFSLITNKCATEY
MsPNP     190 GTYVMLAGPNFETVAESRLLKMLGADAVGMSTVPEVIVARHCGLRVFGFSLITNKVVMDY
HsPNP     190 GTYVMVAGPSFETVAECRVLQKLGADAVGMSTVPEVIVARHCGLRVFGFSLITNKVIMDY

PNP-1a    267 DAS--VEVSHEEVMDIAQQAGERASRFVSDIITEITL-----
PNP-1b    284 DAS--VEVSHEEVMDIAQQAGERASRFVSDIITEITL-----
DmPNP     357 SDKKDDEANHDEVMAVAKNRQKACCELVSRLIREIHLASA--
MsPNP     250 ENL--EKANHMEVLDAGKAAAQTLERFVSILMESIPLPDRGS
HsPNP     250 ESL--EKANHEEVLAAGKQAAQKLEQFVSILMASIPLPDKAS
```

*jy90

S1 Fig

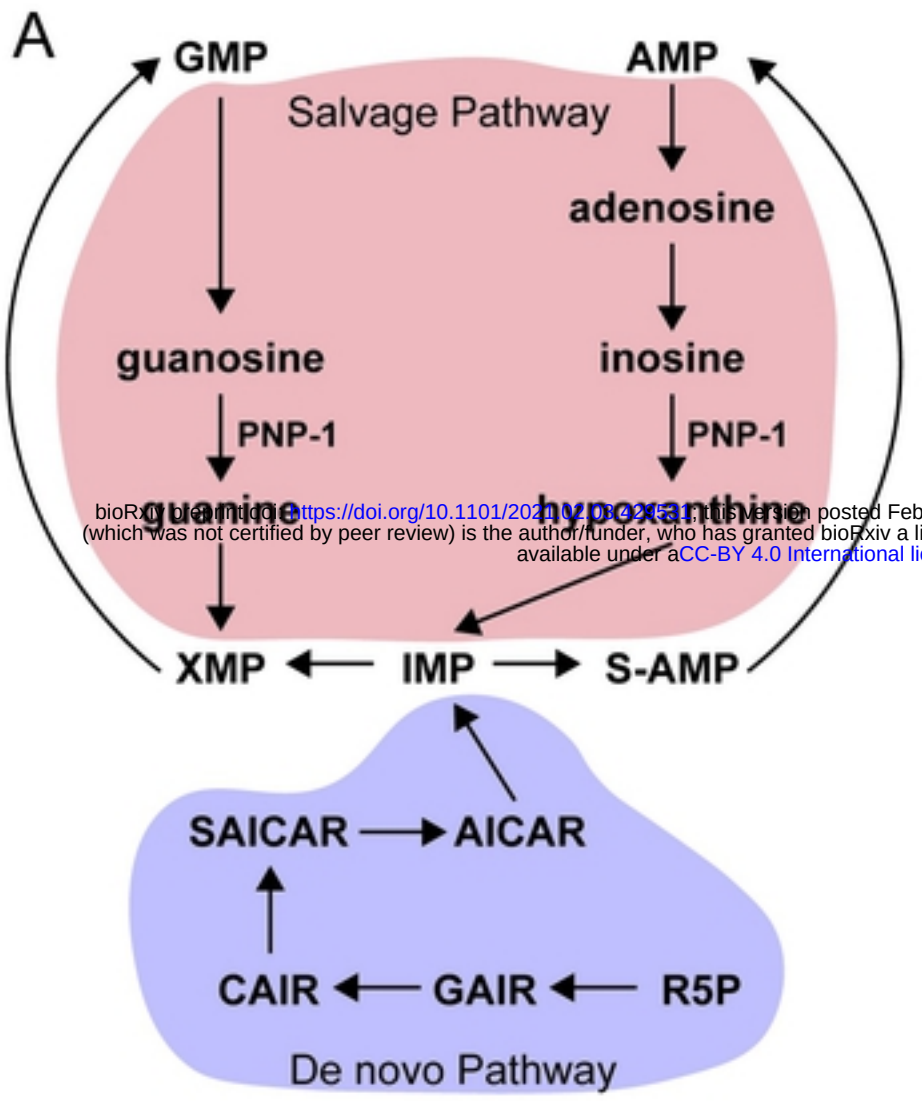

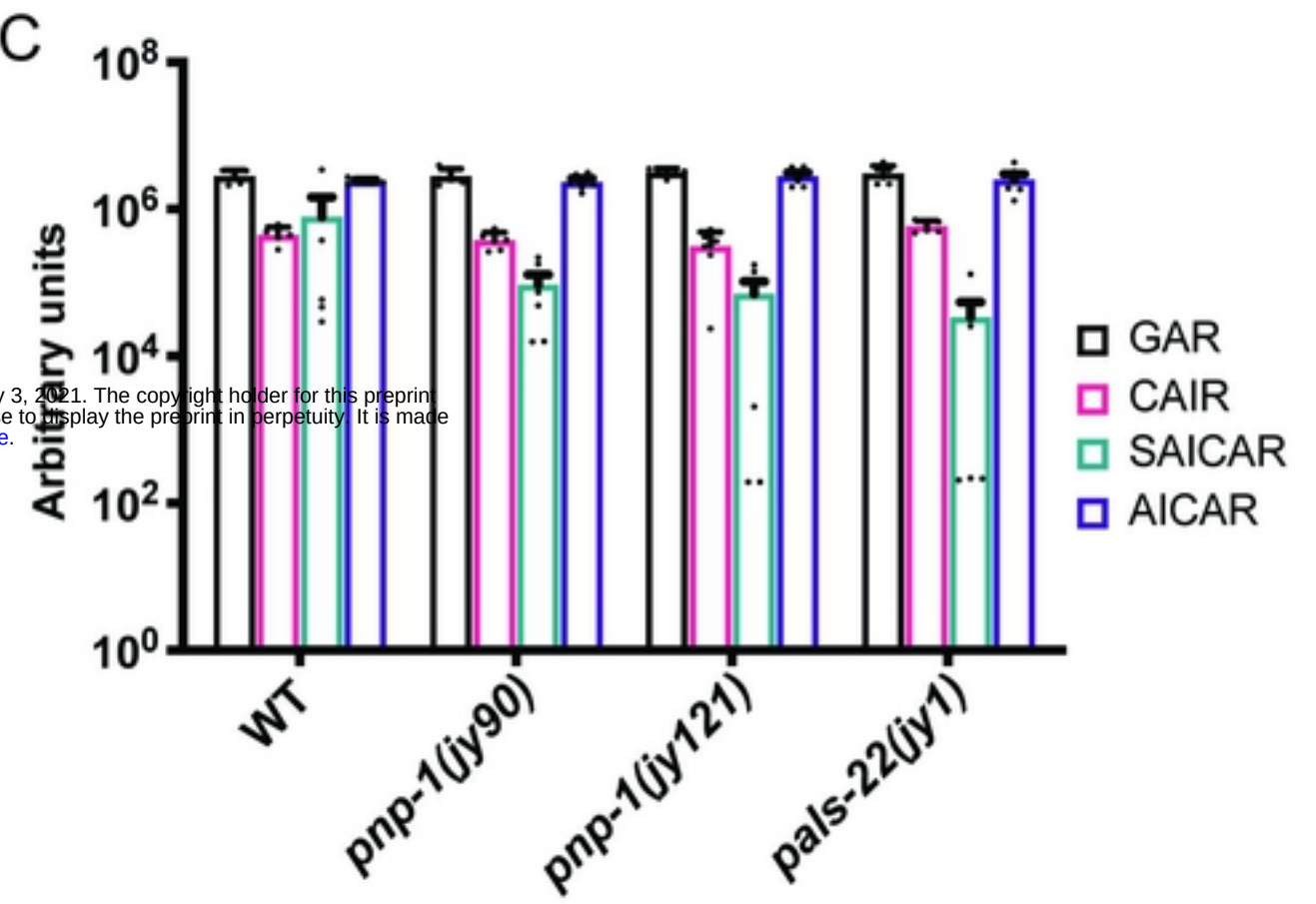

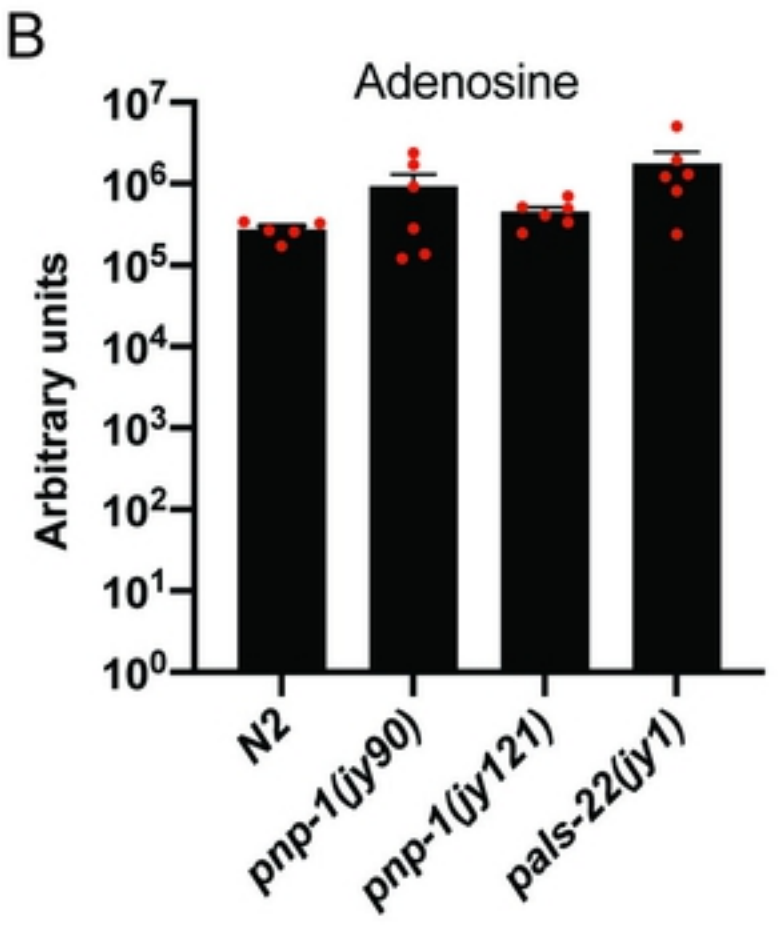

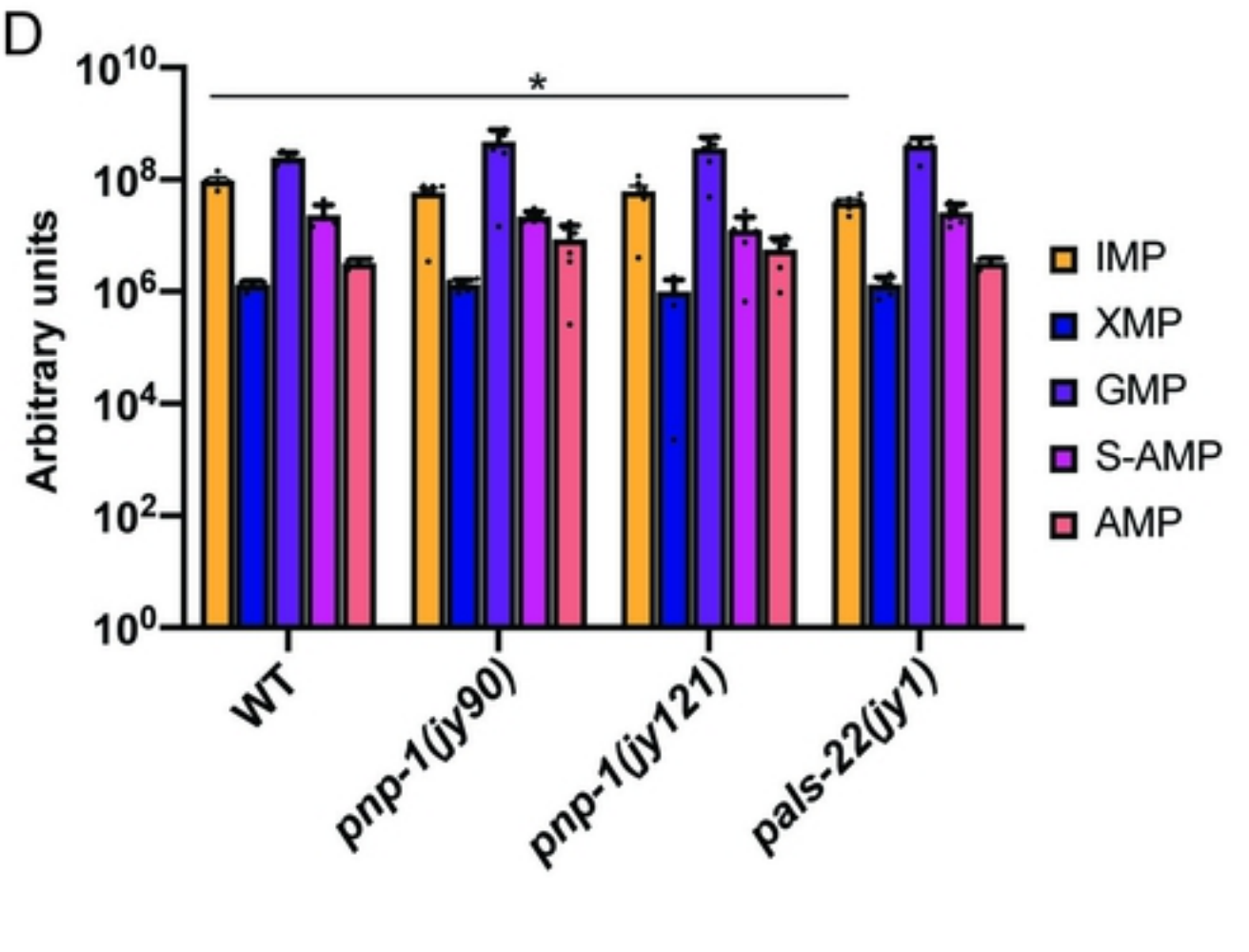

S2 Fig

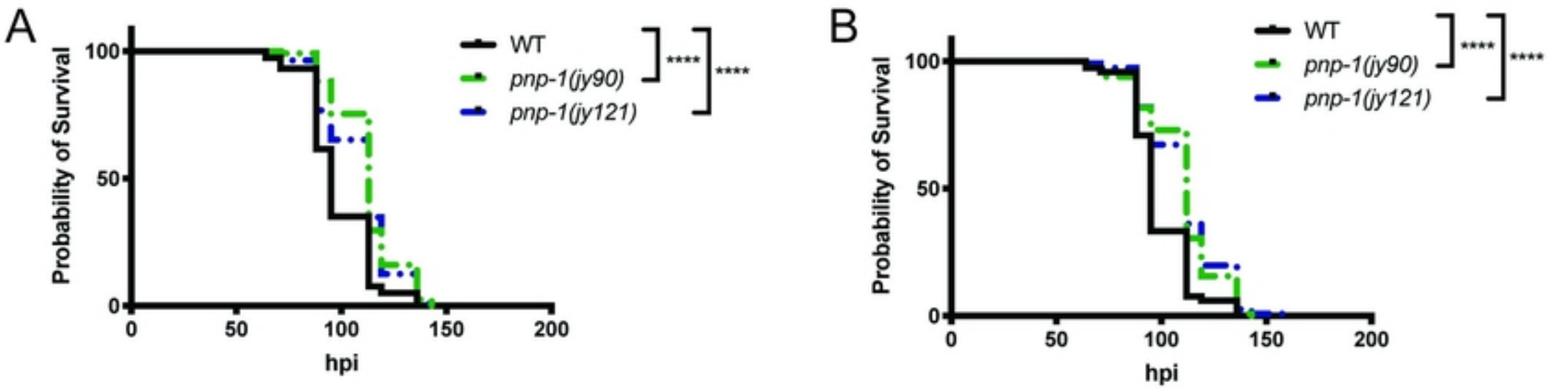

S3 Fig

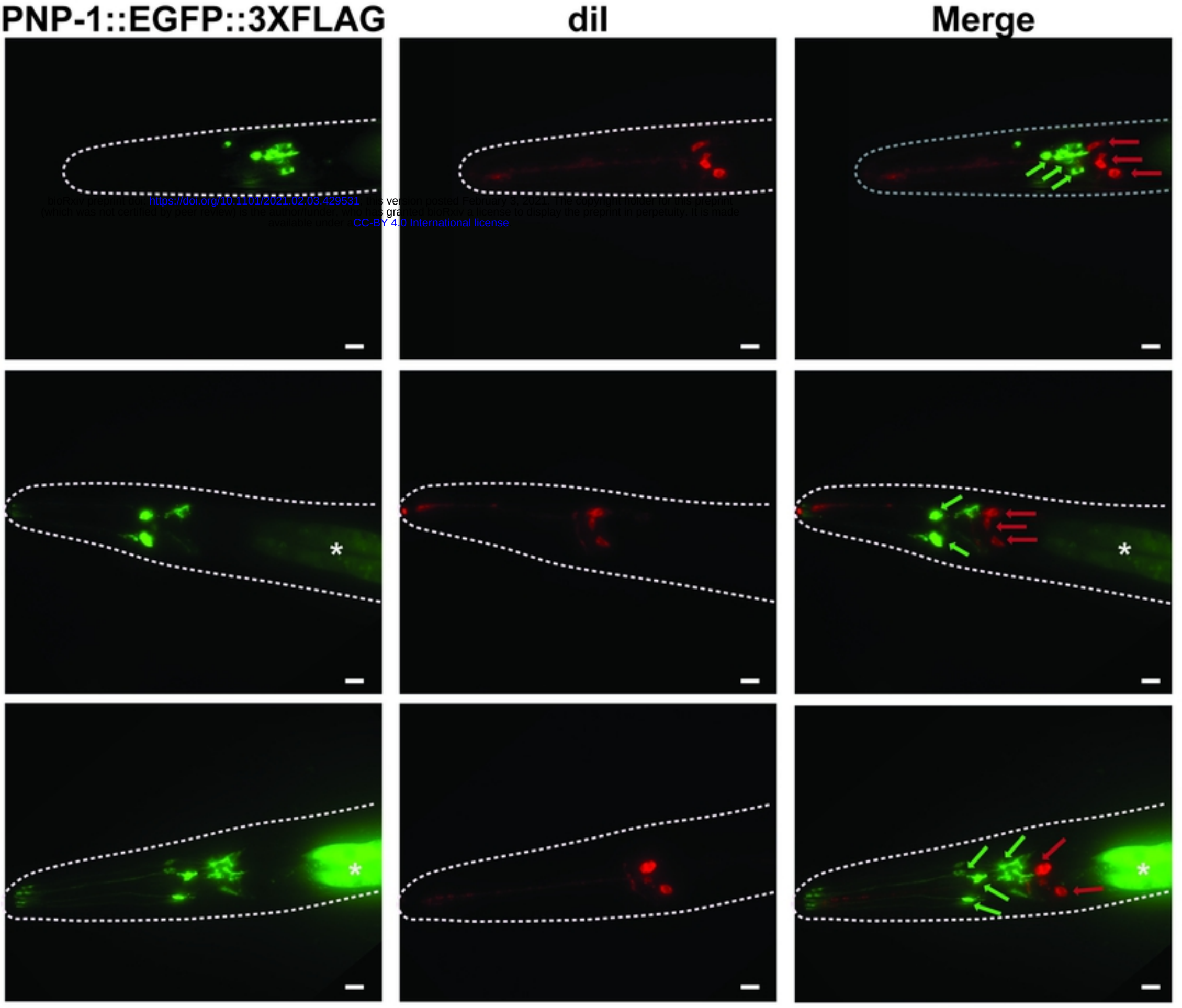

S4 Fig

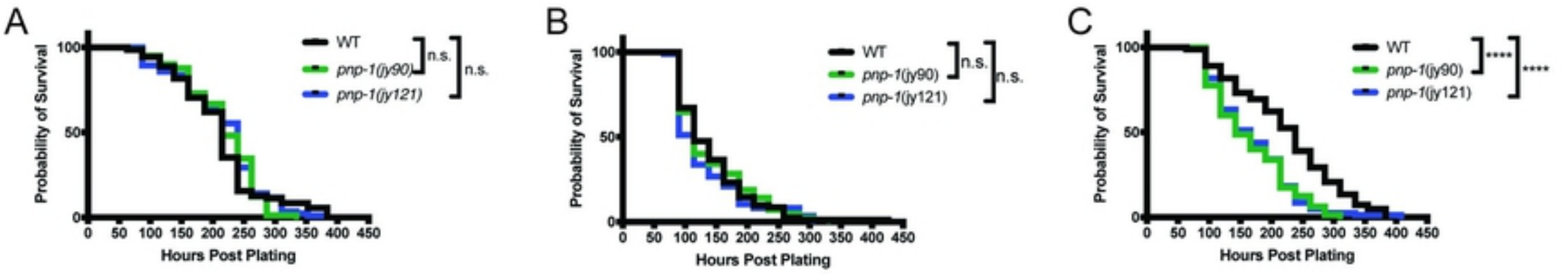

S5 Fig